NCAR TECHNICAL NOTE
NCAR/TN-369+STR
January 1993

# A Revised and Expanded Catalogue of Mass Ejections Observed by the *Solar Maximum Mission* Coronagraph

J. T. Burkepile
O. C. St.Cyr

HIGH ALTITUDE OBSERVATORY
NATIONAL CENTER FOR ATMOSPHERIC RESEARCH
BOULDER, COLORADO

TABLE OF CONTENTS

## PREFACE

This is a revised and expanded catalogue of coronal mass ejections identified in data from the High Altitude Observatory's coronagraph aboard NASA's *Solar Maximum Mission* spacecraft. The list includes events observed during 1980 and the period 1984 through 1989. The first edition of this catalogue was published in July 1990 (NCAR/TN-352+STR). In this edition, descriptions and measurements of mass ejections included in the first catalogue have been expanded and revised (where necessary). A few additional mass ejections have been identified in the data and have been added to the listing. The catalogue has been expanded to include morphological descriptions of each event and apparent speed measurements, whenever possible. We anticipate that many other investigators, including members of other SMM instrument teams, solar observers with associated data sets, and interplanetary researchers will find this list useful.

J. T. Burkepile, January 1993

O. C. St.Cyr, January 1993

High Altitude Observatory

Boulder, Colorado.

# I. INTRODUCTION

The Solar Maximum Mission (SMM) observatory was launched February 14, 1980, from Cape Canaveral, Florida into a 574 km altitude circular orbit inclined 28°.5 to the equator. The ~95 minute period of each SMM orbit was divided into roughly 60 minutes of satellite day and 35 minutes of satellite night. Among SMM's primary science objectives was the study of the dynamics of solar flares and the study of solar magnetic fields associated with the flare phenomenon. SMM's payload consisted of eight instruments that provided broad spectral coverage of radiation produced by solar flares.

HAO provided a white-light coronagraph/polarimeter (C/P) to study the relationship of the corona to the flare process. For a detailed description of the SMM coronagraph/polarimeter instrument and scientific objectives, see MacQueen *et al.* (1980). This instrument obtained data from March through September in 1980 before suffering an electronics failure that rendered it inoperative. A few weeks later, the SMM spacecraft attitude control system malfunctioned, and stable pointing of the spacecraft was no longer possible.

The *Challenger* space shuttle was launched on April 6, 1984, to attempt an in-orbit repair of SMM. That mission was successful in replacing both the spacecraft attitude control system and the coronagraph Main Electronics Box. Details of the retrieval, repair, and redeployment of SMM by the shuttle crew have been documented by Woodgate and Maran (1987).

The coronagraph resumed full operation in June 1984, monitoring the corona during the daylight portion of each orbit. Coronal observations were unavailable from 8-26 January, 1986 due to the loss of memory in the on-board spacecraft computer. Only a few coronal images were obtained between 26 January and 25 February 1986 due to the special observations of Comet Halley. Observations were interrupted in December 1986 when the instrument's dedicated tape recorder failed. Operation was restored in March 1987, with the data being stored on the spacecraft's single remaining tape recorder. This resulted in a degradation of the temporal resolution of the instrument (from 1.5 minutes between successive images before December 1986, to eight minutes between images beginning in April 1987). Observations continued until SMM lost attitude control on November 17, 1989. The spacecraft re-entered the Earth's atmosphere at 10:26 UT on December 2, 1989, over the Indian Ocean (latitude 3.°1 North, longitude 88.°6 East). The coronagraph generated ~240,000 images of the solar corona before its demise.

## II. INSTRUMENT DESCRIPTION

The SMM coronagraph used a complex arrangement of internal and external occulting elements to block out the light from the Sun's disk and to permit imaging of the Sun's outer corona. We will briefly review the important characteristics here.

The telescope produced an image of the corona with a square field of view extending from 1.6 $R_\odot$ (solar radii) to 4.1 $R_\odot$ at the sides and out to just over 6.0 $R_\odot$ along the diagonals. A sector mirror directed the image of one "quadrant" of the corona to the vidicon detector in each exposure. A nearly full view of the corona could be obtained by rotating the sector mirror through four orthogonal quadrant positions. In the normal spacecraft orientation, the south polar region of the Sun's corona was obscured by the shadow of a pylon supporting the occulting disk assembly. The intensity of coronal features within about 20° of the center of this pylon shadow was greatly attenuated. To uncover the south polar regions of the corona, the spacecraft was rolled 90° for a single orbit several times each week. This was done occasionally in 1980 and on a regular basis beginning in 1984.

Images were frequently taken at a high spatial resolution of 6 arc seconds in March 1980 and immediately following the repair in 1984. However, the normal mode of observation produced coronagraph images in low resolution mode, wherein the spatial resolution (pixel size) was 12 arc seconds.

The instrument package contained several spectral filters to meet mission objectives. Most of the coronagraph images were obtained through a wideband filter in the "green" portion of the visible spectrum (half-power bandpass 500 nm - 535 nm). During 1980, images were occasionally obtained through a very narrow bandwidth interference filter (530.0 nm - 530.6 nm) containing the forbidden emission line of Fe XIV. Two coronal mass ejections have been identified in this bandwidth in the 1980 data set and are noted in the event list. Prior to 1987, a limited number of images were also obtained through a narrow bandpass filter (654.3 nm - 658.3 nm) centered on the H$\alpha$ emission line of neutral hydrogen.

Three polarizing filters (with polarization planes oriented at 60° angles) were used to analyze the polarization of the observed radiation, both on a daily basis for synoptic purposes and (when activity warranted) intermittently several times per day.

The "duty cycle" for detection of coronal mass ejections by this instrument during the 1980 operations was quantified by Hundhausen *et al.* (1984) and was based on the average speed of mass ejections through the telescope's field of view. A minimal observing cycle for detection of most mass ejections required that at least one complete set of images in the

four quadrants be obtained during each 95 minute SMM orbit. During the 1980 operations, a selected quadrant was often observed for a prolonged period following a flare alert. As a result, images of the other three quadrants were not obtained. The 1980 duty cycle for mass ejection detection was quite low. Only 28% of the orbits imaged all four quadrants.

With the resumption of observations in 1984, a change of observing philosophy was instituted, and nominal operations included at least one complete set of images from three quadrants (north, east, west) during each orbit. The south quadrant was added to this nominal sequence in August, 1984. The instrument's duty cycle for all years following the 1984 repair was quite high, with complete coverage averaging 78% of the available orbits each year. (Annual values for the duty cycle have been published by MacQueen and St.Cyr, 1991.)

Following the 1984 repair, the instrument experienced sporadic periods of degraded image quality. The degraded images appear to have dark and bright horizontal streaks randomly placed throughout the image. The streaking problem appeared for periods ranging from a few minutes to several weeks, and the effects on identification of features such as mass ejections ranged from minor to severe. The horizontal streaking was probably caused by an onboard electronics problem; however, no correlation with any operational or environmental parameter was ever discovered. (Photographic examples of horizontal streaking in the data are shown in upper right photo in Figure 8a on page 25, the lower left photo in Figure 16 on page 41 and in the two lower photos on page 49.)

## III. IDENTIFICATION OF MASS EJECTIONS

Hundhausen *et al.* (1984) defined a coronal mass ejection as:

> "...an observable change in coronal structure that (1) occurs on a time scale between a few minutes and several hours and (2) involves the appearance of a new, discrete, bright, white-light feature in the coronagraph field of view."

Those authors note that this definition is virtually identical to that used by Munro *et al.* (1979); however, an additional requirement for the present catalogue has been that these new features should display a predominantly outward motion through the field of view, as in the definition used by Howard *et al.* (1985) in the identification of mass ejections in the Solwind coronagraph. In a few cases (less than 1% of all mass ejections), we observed the addition of new material into the corona in one image only. The material was gone from the field of view in the next availale image. It was, therefore, impossible to view outward motion. Of the remaining 99% of identified ejections that were visible in more than one image, none

showed conclusive evidence of coronal material falling sunward. We have noted one event in 1989 that contained suspected prominence material observed to fall back through the field of view. Since all events visible in multiple frames showed outward motion only (except the one prominence case noted), we identified single image events as mass ejections. We have noted in the 'Comments' column if the event was visible in one image only. (NOTE: This is different from the FRONT of a feature being visible in one image only)

Candidate mass ejections for this event list were identified by examination of the data on a video display. Consecutive images were "toggled" (blink comparison) and changes in the corona were (most often) readily apparent to the viewer. Less frequently, images were digitally subtracted pixel-by-pixel from an earlier base image, thereby enhancing faint or subtle changes occurring during the time between the images.

At present, we have not rigorously quantified the brightness threshold for detection of mass ejections. We believe that the instrument sensitivity was generally sufficient to allow detection of enhancements (or deficits) of about 10% above (or below) the pre-event background. A photographic example of a very faint event is given in Figure 20a on page 49. We note that it is most often the apparent outward motion of new features when viewed in sequential images that indicated the presence of a mass ejection.

A small percentage ($\sim$ 8%) of events are listed as multiple-part phenomena. These events are counted as **one** event in the total number of events for any given year. We used the following guidelines in determining multiple-part events: (i) a succession of ejections occur at or nearly at the same position angle over a period of hours; (ii) multiple, overlapping or immediately adjacent ejections occur nearly simultaneously; (iii) a much smaller ejection occurs in the general vicinity and time as a larger event. There is a degree of subjectivity involved in deciding if ejections are multiple-part or multiple events, and it becomes increasingly difficult to resolve events when activity is high. We note that there are approximately twice as many multiple-part events reported during years of maximum activity than at solar minimum.

The mass ejections listed here comprise a subset of all observable changes in the corona. Assignment of events to any such list involves some subjective judgment, but an entry in this catalogue signifies that at least two individuals agreed that a temporal change in the visual appearance of the corona met our definition of a mass ejection. Those changes not meeting the definition described above have been deemed "anomalies" and have not been included in this listing. In addition, if an event was completely missed (*i.e.* dramatic changes occured in the corona during spacecraft night or a data gap), it has not been included in

this catalogue but instead has been mentioned in the anomaly listing. (Information about specific coronal anomalies is available upon request.) All SMM coronagraph data have been systematically surveyed twice, and this list is complete as of January 1993.

Detailed tabulation of coronal mass ejections and their properties for the 1980 and 1984 through 1987 observations have been circulated to investigators in the past. The deluge of events in 1988 and 1989 (accounting for more than 70% of the total number of mass ejections observed by SMM) precluded formation of a detailed listing of properties in a timely manner. Instead, we chose to circulate a preliminary catalogue documenting times, locations, widths, and a brief description for each event identified at that time (St.Cyr and Burkepile, NCAR/TN-352+STR, July 1990). The present publication should be considered a "revised and expanded" version of that catalogue which: (1) refines and corrects information in the first catalogue; (2) includes a few additional mass ejections identified since publication of the first catalogue; (3) includes apparent speed measurements where possible (about half of the mass ejections); and (4) includes more precise descriptions of mass ejection morphologies. Detailed information on individual events will be made available upon request.

## IV. DESCRIPTION OF THE CATALOGUE

We have included twelve columns of information in this catalogue. The first five columns list the date, day-of-year, time, central location and width. The next six columns list information on the apparent motion of the ejection and are grouped under the heading 'Kinematics'. The last column gives a brief description of each event. Detailed descriptions of the methods and definitions used to derive the information listed in the tables are given below.

### A. Date, DOY, Time[UT]

Each page in the event list is identified by year. Within a given year, each event is identified by both the calender date(s) and the day(s) of year (DOY) on which it was observed. The column 'Time' lists the Universal Times of the first and last image on which the event is visible in the instrument's field of view. If the event spans more than a single date, then the first time listed corresponds to the first date and the second time listed correspond to the second date. In some instances, there is a judgment required as to when a mass ejection begins and ends. More often, the stop time is difficult to determine. We have attempted to list the stop time as the first image in which all outward flow of material from the field of view has ceased. The start time is subjective for those cases when a slow expansion or brightening evolves into a mass ejection. These less certain times are designated

by a '~' or '?' in the listing.

NOTE: A discrepancy was found late in the mission between the spacecraft's onboard clock and Universal Time. The error was cumulative over the life of the mission and was correctable. Data taken in 1980 had to have a few seconds added to it to correct the times. By 1989, approximately three minutes needed to be added to the image times to correct them. Times reported in our previous catalogue (1990) were **not** corrected. **ALL** times reported in this catalogue have been corrected.

### B. Central Locations

Mass ejection locations are given as a function of position angle (PA) and are measured in the conventional sense from solar north through east. The central angle (Ctrl PA) has been taken to be the geometric center between the two outermost sides of the identified feature. All position angles quoted in this catalogue are projected onto the plane of the sky. Projection of off-limb, non-equatorial features produces an overestimate of the actual latitude. No attempt has been made to correct for this effect. (See Appendix B of Hundhausen (1993) for a discussion of projection effects.)

### C. Apparent Widths

Angular widths were determined by the method described by Hundhausen (1993) and St.Cyr and Burkepile (1990). The position angles of the two outermost sides of a feature were located at the lowest altitude at which reliable measurements could be made (typically 2.0 to 3.0 $R_\odot$). Measurements were made at a time and height when the features had expanded to their maximum width. Obvious deflections of adjacent pre-existing coronal features have not been included in the width determinations. If the edge of a feature was obscured from view (e.g. by the pylon shadow, or by sector mirror field of view limitations), the position of the outermost visible edge was noted. Widths and central positions of such events are marked with '>' or '<' signs, and have not been included in the histograms.

In most instances, only one central angle and width are denoted for a given event. These measurements always refer to the widest feature comprising that event. Apparent width measurements should be accurate to $\pm$ 5° unless otherwise designated by a '~' or '?'. The overestimation of latitudes of off limb features will add to the overall uncertainty of width and central position angle determinations. The resulting histograms of these quantities reflect these uncertainties. No attempt has been made in this catalogue to correct for these effects. A more detailed discussion of projection effects on width and latitude distributions will appear in the future.

## D. KINEMATICS

We have attempted to quantify the outward motion of identified features comprising each event. A brief description of the six columns of trajectory information follows.

### 1. Trajectory Times

The times when the height measurements of a feature were made are given in the trajectory times column. These include only those image times used to construct the trajectory that determined the preferred speed. (Preferred speeds are discussed in the next section.) Trajectory times are a subset of the event times listed in column three. In a number of instances, the ending time in the 'Trajectory Times' column is much earlier than the event stop time. This is due to the fact that material continued to be ejected through the field of view long after the front was gone.

### 2. Apparent Speeds

Speeds are given in kilometers/second and are apparent speeds as projected onto the plane of the sky. Speeds of off-limb features will be underestimates of the actual value. No correction for projection effects has been attempted. We measured apparent radial distance from sun center in each image. In many events, we were able to measure more than one feature per event. Speeds of all measured features are presented in the tables.

We occasionally made multiple speed determinations for a single feature by taking measurements at different position angles or by excluding from the trajectory one or more less reliable data points. Speed measurements of a single feature varied due to changing acceleration rates and/or non-radial motion. When multiple speed determinations of a single feature were available, we used the following criteria for inclusion in this catalogue: (i) we chose the speed measurement with the highest quality parameter (described below); (ii) if quality parameters were equal, we chose the speed measurement with the most data points used in the determination; (iii) if quality and number of points were equal, we chose the speed measurement nearest the central position angle.

Error bars (typically $\pm$ 0.1 to 0.2 $R_\odot$) were assigned to each data point when the measurements were made and were used in the least squares fitting procedure. Error bar estimates were based on the following: (i) the sharpness of the feature; (ii) the change in position of the occulting disk diffraction pattern between images (reflecting the error in the standard coordinates used to mark the center of the occulting disk and sun center); (iii) the use of images from different sector mirror settings; (iv) the overall image quality (*i.e.* severity of electronic artifacts and horizontal dark streaking); (v) the ability to follow a given

feature from image to image. Most height determinations were made using direct images, but occasionally pixel-by-pixel subtractions from a pre-event base image were necessary to determine the location of faint features.

We have chosen not to report an uncertainty for speed measurements. Although we obtained a quantitative measure of this uncertainty from the least squares fitting of the data, there were other factors involved that added to the uncertainty. Some factors, such as the location of a feature out of the plane of the sky, were impossible to determine. The quality rating (discussed below) indicates our confidence in determining speeds. A 20% uncertainty can cautiously be applied to a speed measurement with an average quality rating (6-7). Lower quality measurements would have a larger uncertainty.

If more than two data points were available, both constant speed (first order least squares) and constant acceleration (second order non-linear least squares) fits were made to the data. In most of these cases, both the constant speed (subscript$_1$) and the final speed (subscript$_2$) are listed. The final speed is defined as the speed determined from the constant acceleration fit, evaluated at the final data point in the trajectory. The authors have chosen a preferred speed and indicated it with a '$\star$'. For trajectories with two data points only, the constant speed is the preferred speed by default. If both a constant speed and a final speed from a second order fit were available then the preferred speed was chosen by a visual inspection of the trajectory fits to the data and by a chi-squared analysis of the fits. In most cases, the first order (constant speed) fit was preferred, fitting all the data points well within each error bar. Of the trajectories with three or more data points, the second order (constant acceleration) fit was clearly preferrable in ~20% of the cases. Approximately 95% of the preferred second order fits exhibited acceleration.

In some events, a very gradual rise of a feature was followed by a rapid acceleration. In these cases, we have excluded from the fit all the data prior to the acceleration in order to get a better estimate of the final speed. An example of such a trajectory is given in Figure 7a on page 23. There are a few cases of three or more data point fits that list either the first OR second order fit speed. We excluded the second order speed in those cases where data points were clustered together in time, effectively behaving like a two-point fit. An example is shown in Figure 7b on page 23. We excluded the speed from a first order fit in those cases where there was a dramatic acceleration (deceleration), in which case the first order fit was a poor description of the measured trajectory. An example of such a trajectory is shown in Figure 7c on page 23.

We caution the reader against comparing speeds of various features within a given

event. Although the different features pass through the same range of altitudes above the solar limb, they have often been measured at different times during the course of an event. Trajectories of specific events are available upon request.

### 3. Speed Position Angle

The position angle at which we measured trajectories is given in the Speed PA column. We attempted to measure features near the apparent central axis of the event, but in some cases, we were forced to choose another position angle within the event because of electronic artifacts, clarity of the feature being measured, etc. The reader may gauge our success in this effort by noting the difference between the central position angle and the position angle of the speed measurement.

In most cases, material was moving more or less radially outward from the sun. Whenever possible, we measured features (including non-radially moving material) at a fixed position angle. A small percentage of the time (~13%) we were unable to follow a feature along a fixed angle and for these measurements we have listed the average position angle used, followed by a '†'. Measurements with varying angles do not necessarily indicate non-radial motion of material. Occasionally a feature may have been obscured at a given angle in one or two images by an electronic artifact. For some events, data was only available in different sector mirrors, and no angle containing the event common to both sectors existed. In ~78% of all non-radial measurement cases, the angular changes did not exceed ± 5°. For all cases, only the apparent radial component of the speed is reported.

### 4. Number of Data Points

The number of data points defining a feature's trajectory is reported in column nine.

### 5. Quality

The quality of the speed measurements is listed in column ten. This does not refer to the quality of the least squares fit to the data, but instead conveys our judgement of the overall quality of the measurements themselves. Quality determinations are meant to assist the user in the utilization of the information given for either a specific event or for use as a comparision for relating speed information between events. The quality of each speed measurement is ranked from 0 (not measurable) to 10 (a perfect measurement, which does not exist). Milestones on this scale are: 1 - measurement may be possible, but speed would be very unreliable; 3 - poor; 5 - mediocre; 7 - okay; 9 - best. Quality is based on several factors, including: (i) the clarity and sharpness of the feature being measured, and its contrast with respect to the background; (ii) our confidence that a measured feature was

identifiable in sequential images; (iii) motion of the feature between the first and last frames was significantly greater than the error bars of the individual points; (iv) the size of the error bars on the individual data points; and (v) the severity of electronic artifacts and horizontal dark streaking in the images.

### 6. Feature

The feature column lists the morphological feature whose central position angle, width, and/or speed was measured. In those cases where we were unable to measure the speed of a feature (quality = 0), we have given an explanation for its immeasurability (eg. no clear front). Unless otherwise noted in the 'Feature' column, all speed measurements were made of the outward expansion at the feature's leading edge.

## E. Comments

The final column in the table is the 'Comments' column. Here we have included morphology information for all events. A list of morphology types is given in the next section. Photographs of the various morphologies are given in a rogue's gallery beginning on page 25. An analysis of various event quantities by morphology will appear in the future. In addition to morphologies, we have attempted to record the following conditions as they relate to pre-existing coronal structures: (i) superposition of features; (ii) deflections; (iii) disruptions and blowouts. Photographs of these phenomena appear on pages 49 through 53. There is a degree of subjectivity involved in determining conditions (ii) and (iii). We have defined deflections as the azimuthal motion during an event of a pre-existing coronal structure away from the event center. By toggling pre-event and event images, we were able to detect deflections greater than $\sim 3^{\circ}$. A pre-existing structure was considered to be disrupted if it survived the event but had undergone a 'significant' change to its shape, brightness and/or location. A blowout is defined as the apparent disappearance of a pre-existing structure following the passage of an event.

In reviewing a data set of this size, it is likely that we have neglected to note some event effects on pre-existing structures. In addition, this data is insensitive to deflections perpendicular to the plane of the sky or to effects by events on pre-existing structures far from the limb. For these reasons the total number of deflections, disruptions and blowouts should probably be considered a lower limit to the actual value.

We have also attempted to give the reader any other relevant (usually non-quantitative) information about the event. For example, we may not have been able to measure a speed for an event, but we would include the word "slow" in the comments,

indicating that the speed was <100 km/s.

Major lapses in temporal coverage of more than one orbit (~95 minutes) are also included in the comments column. These "data gaps" are arranged chronologically with respect to the mass ejection entries. No data exists between the times listed in the data gap entries.

## V. DESCRIPTION OF APPARENT MORPHOLOGIES

We have attempted to describe the distribution of new material within each mass ejection. We have not followed the classification scheme presented by Munro and Sime (1985) for the mass ejections detected by the *Skylab* coronagraph, nor have we used that of Howard *et. al.* (1985) for events detected by *Solwind.* Those authors characterized each mass ejection as belonging to one of several classes. We note that a variety of morphological features may be present during the evolution of a mass ejection. We have attempted to record ALL of the morphologies seen within each mass ejection.

A morphological scheme is at best highly subjective. Often features do not fall neatly into one category. The shapes of features may evolve as they move outward through the corona or may be altered due to projection effects if they are moving out of the plane of the sky. The classification task was difficult (to impossible) for some mass ejections because: (a) there was poor contrast of the new material with respect to previously existing coronal features, or the vidicon detector background levels fluctuated between images; (b) the material evolved from image-to-image; (c) the new material was poorly placed within the field of view (*e.g.,* electronic artifacts, pylon shadow, or sector mirror boundary); or (d) the event was in a limited number of frames or was interrupted by a data gap. Consequently, some mass ejections are described in this catalogue simply as 'material.'

We have not attempted to quantify our certainty of a feature falling into a given classification. In less certain cases, we have included a '?' or listed an alternative morphology in parenthesis in the comments column [*e.g.* loop/cavity (or mound) ]. Morphologies mentioned in parenthesis are **not** included in any morphology tables or histograms.

Caution should be used when comparing reported morphologies from other data sets. Instruments will vary in their sensitivity and field of view. Different data processing and visualization techniques used in the analysis may favor (or discriminate against) certain morphologies. We note, however, that there exist morphologies common to all coronagraph data sets. It has been noted by Munro and Sime (1985) and others that morphologies may offer clues to the circumstances surrounding the origin and propagation of mass ejections

and their associations with other solar activity. In this spirit, we believe it is important to include the statistics of morphologies in this catalogue. A more extensive report of physical quantities related to morphology will appear in the future.

The following list presents the eleven morphological features identified in SMM mass ejections. Occasionally, features possessed additional geometric characteristics or displayed a high degree of internal structure worthy of record. In order to avoid counting the same feature in multiple morphology categories, we made use of five descriptors to further categorize events. Descriptors are listed following the morphology definitions. For example, a flat-topped, light-bulb-shaped loop/cavity will appear only once in the morphology listing in Table 2 under loop/cavity. In addition, one entry was made in both the light-bulb and flat-top descriptor categories in Table 3. All features were recorded in one of the eleven morphology categories. Thus, Table 2 accounts for 100% of all features mentioned in the 'Comments' section of the mass ejection catalogue. Morphologies and descriptors are listed below according to their relative frequency of appearance.

## MORPHOLOGIES

**LOOP/CAVITY** — We propose that the appearance of the well-known "frontal loop" in a mass ejection is actually evidence of "a loop and trailing cavity" since the region immediately following the loop is (by definition) fainter than the loop. In fact, this "cavity" along the back edge of a "loop" is frequently better defined than the leading edge of the loop. Unless otherwise noted, we interpret frontal loops to be composed of coronal material. We have attempted to distinguish between "outer" versus "inner" loops, and if multiple loops are present, we have attempted to note whether they were "concentric" or "overlapping". Multiple loops/cavities accounted for 12% of all loops.

**CORE** — It is not uncommon to detect a bright central region (often amorphous) in the dark cavity trailing a front. We have defined this material to be a core. By definition, a core indicates the presence of a cavity to distinguish it from the front. A core is **never** the leading feature. Cores are almost exclusively associated with the loop/cavity morphology.

**CLOUD** — Clouds are faint, amorphous distributions of new material, spanning several tens of degrees in width. Clouds usually have a hint of a curved front and may be thought of as ill-defined mounds.

**GENERIC MATERIAL** — We have used this classification to refer to complex, very ill-defined features that do not fall into any one category.

**MOUND** — The tops of mounds often have a well-defined, curved appearance similar

to the frontal loop, but there is no obvious decrease in brightness behind the leading edge (*i.e.*, no apparent cavity). In a few instances, we detected cavities or bright cores embedded within a mound, but most often, a mass ejection with this classification was featureless. Note that digital subtraction (differencing) of successive images of a mound or filled front could falsely lead to a "loop/cavity" classification. The photo in the upper left corner of Figure 11a on page 31 is a differenced image of a mound that could be mistaken for a thick loop followed by a cavity. It was clearly visible in direct images as a mound and was recorded as such in the morphology table. Direct images should be used (or if differencing is necessary, a pre-event base image must be used) to properly classify this type of mass ejection.

**CAVITY WITH NO LOOP FRONT** — We have detected rarefactions (dark voids) that appear to move through brighter regions (*e.g.,* helmet streamers) of the corona without a detectable frontal loop preceding them. If a front is present, it is not bright enough to be visible above the background corona.

**BLOB** — These are smaller, often narrow, self-contained regions of new material. Blobs usually have well-defined boundaries and little or no inner structure. They are often seen as part of a larger distribution of new material.

**JET** — These are narrow (less than ~ 20° wide), featureless appearances of new material and usually have ill-defined fronts, but well-defined sides.

**TONGUE** — A "tongue" has more-or-less constant breadth and often has a curved shape. Like jets and fans, the sides are usually more sharply defined than the front. Tongues tend to be narrow, but can be greater than ~20° wide.

**STREAMER EVENT** — A streamer event is the disruption or blowout of a pre-existing helmet structure with no obvious ejection of new material or features (including cavities) distinct from the streamer. The helmet streamer maintains its identity throughout the event. Streamer events are often characterized by an initial brightening and/or slow swelling (in both the azimuthal and radial directions) of the streamer. In other cases the streamer elongates outward. Disappearing streamers that exhibited a gradual swelling prior to their ejection are discussed (and termed "bugles" ) by Hundhausen (1993).

**FAN** — Like jets, fans tend to have ill-defined fronts but do have well-defined lateral edges that extend more-or-less radially. Fans vary in width from very narrow to 90° wide.

## DESCRIPTORS

**PROMINENCE** — We have identified a small percentage of mass ejections as

containing "prominence" material. This interpretation is certainly warranted when the material was observed to be bright in images obtained through the instrument's H$\alpha$ emission filter. But in many cases where no H$\alpha$ data exists, the identification of prominence material has been based on the knotty or highly structured appearance of at least part of the new feature(s) in the mass ejection. These "prominence" features differ significantly from the often amorphous appearance of coronal material. Since this is an interpretative description, we have used parentheses with the word "prominence" when we suspect its appearance. We note that the appearance of prominence material occurred more frequently during years of maximum activity.

Since prominences expand and may become more ionized as they move away from the solar disk, they are likely to lose the highly structured and organized appearance that identifies them. For this reason, the number of possible prominence features reported here is probably a lower limit. In addition, we note that most of the features identified as prominences trailed behind a coronal front. This configuration was reported by Hildner *et al.* (1975) and Schmahl and Hildner (1977) in the *Skylab* data set.

**CONCAVE-OUTWARD** — Concave-outward refers to the geometry (most often 'U'- or 'V-'shaped) that opens away from the sun. (In contrast, most "loops" are concave toward the Sun.) We have resisted the temptation to refer to these as 'disconnections' since there are a variety of interpretations of such features in the literature. Examples have been described by Illing and Hundhausen (1983), Webb and Cliver(1989), and McComas *et al.* (1991). These suspected 'disconnections' certainly fit the criteria for "mass ejection," since they showed apparent outward motion. A number of these structures have been detected in the late stages of a mass ejection.

**FLAT-TOP** – The term "flat-topped" is self-explanatory. This geometry may indicate the presence of a slow shock as described by Hundhausen *et al.* (1987).

**LIGHT BULB** — This geometry is almost exclusively associated with the three-part structure of loop/cavity and core. It refers to the "ballooning" of the lateral boundaries of the loop (*i.e.*, the width increases with increasing altitude).

**HALO** — Although there are several possible "halo" events identified in the listing, we have not observed the morphology described by Howard *et al.* (1982): "a halo of excess brightness completely surrounding the occulting disk and propagating radially outward in all directions from the Sun." Instead, the halo events we have identified are either events possessing very large widths ($> 120°$) or the appearance of multiple mass ejections at several

position angles, apparently occurring nearly coincidentally.

## VI. HISTOGRAM AND TABLE DESCRIPTIONS

To complement this catalogue, we provide graphical presentation of several measured quantities tabulated in this publication. For a contextual view of early SMM results and results from other instruments, the reader is referred to other reviews (e.g., Kahler, 1987). The central position and width histograms reported in this technical note do not differ greatly from our original report [St.Cyr and Burkepile, 1990].

Mass ejection totals are tabulated in Table 1. We have included total number of mass ejections, central position latitudes (converted from central position angles), widths, and speed information. We have listed the percent occurrences, by year, of identified morphologies in Table 2 and descriptors in Table 3. All tables appear on page 16.

The distribution of apparent locations of the mass ejections observed by SMM is shown for individual years in Figure 1 on page 17, and for all years combined in Figure 2 on page 18. Here we have plotted the central position latitude of all measured features.

One conclusion is immediately obvious from Figure 1. The events detected in the years of solar activity minimum conditions (roughly 1984 through 1987) are strongly clustered near the Sun's equator. As Hundhausen (1993) has noted, this clustering of mass ejections near the heliographic equator at solar minimum phase can be even more pronounced when viewed in heliomagnetic coordinates (as in 1984). It is only during more active phases of the sunspot cycle that a significant fraction of mass ejections are detected at apparent latitudes approaching the Sun's poles. The composite graph of all years' data (Figure 2) is of course dominated by mass ejections occuring in 1988 and 1989.

The distribution of measured widths for the mass ejections is shown in Figure 3 on page 19 for individual years, and in Figure 4 on page 20 for all years combined. Since there are so few events with widths greater than 120°, we have intentionally truncated the graphs at that value. We do not see appreciable changes in width distributions with solar cycle.

The speed distribution for all measured features is shown in Figure 5 on page 21 for individual years, and in Figure 6 on page 22 for all years combined. Speeds spanned approximately three orders of magnitude (from under 10 km/sec to over 2000 km/sec). Because there are so few features with speeds greater than 1200 km/s, we have chosen to truncate the plot at that value. A detailed discussion of the statistics of mass ejection speeds and accelerations will appear in the future.

# TABLE 1: SMM Coronal Mass Ejection ANNUAL TOTALS

| | | Apparent Latitude | | | Apparent Widths [°] | | | Apparent Speeds [km/sec] | | |
|---|---|---|---|---|---|---|---|---|---|---|
| YEAR | # of CMEs | Avg. | Std. Dev. | # Features Measured | Avg. | Median | # Features Measured | Avg. | Median | # Features Measured |
| 1980 | 169* | -0.3 | 42.2 | 227 | 39 | 36 | 210 | 355 | 298 | 135 |
| 1984 | 62 | 6.0 | 31.4 | 69 | 44 | 40 | 68 | 157 | 123 | 43 |
| 1985 | 57 | 0.5 | 18.3 | 60 | 50 | 42 | 60 | 458 | 235 | 39 |
| 1986 | 60 | 2.6 | 12.8 | 65 | 46 | 42 | 63 | 371 | 285 | 62 |
| 1987 | 117 | -2.6 | 22.4 | 123 | 44 | 42 | 115 | 262 | 236 | 118 |
| 1988 | 379 | 1.7 | 33.1 | 435 | 52 | 50 | 404 | 322 | 263 | 241 |
| 1989 | 507 | 2.3 | 38.7 | 590 | 45 | 40 | 542 | 410 | 357 | 298 |
| TOTAL | 1351* | 1.5 ° | 35.0° | 1569 | 46° | 42° | 1462 | 349[km/s] | 285[km/s] | 936 |

*includes two events visible only in the narrow bandwidth containing the forbidden emission line of Fe XIV.

# TABLE 2: SMM Coronal Mass Ejection MORPHOLOGIES

| | Percentage of All Morphologies | | | | | | | |
|---|---|---|---|---|---|---|---|---|
| MORPHOLOGY | 1980 | 1984 | 1985 | 1986 | 1987 | 1988 | 1989 | TOTAL |
| Loop/cavity | 32.4 | 27.2 | 26.4 | 37.8 | 31.7 | 28.5 | 35.3 | 32.1 |
| Core | 15.4 | 19.6 | 14.9 | 23.5 | 15.8 | 15.6 | 16.9 | 16.5 |
| Cloud | 11.8 | 8.7 | 11.5 | 10.2 | 11.5 | 14.1 | 20.1 | 15.4 |
| Material | 9.5 | 12.0 | 17.2 | 12.2 | 13.7 | 13.2 | 8.1 | 11.0 |
| Mound | 11.5 | 10.9 | 6.9 | 5.1 | 12.0 | 10.3 | 7.6 | 9.2 |
| Cavity (No Loop) | 4.6 | 4.3 | 5.8 | 2.0 | 6.6 | 4.5 | 2.6 | 3.9 |
| Blob | 4.3 | 2.2 | 2.3 | 3.1 | 1.1 | 3.2 | 3.0 | 3.0 |
| Jet | 4.6 | 3.2 | 2.3 | 1.0 | 2.7 | 3.2 | 1.9 | 2.7 |
| Tongue | 3.6 | 0.0 | 0.0 | 0.0 | 0.5 | 3.9 | 2.7 | 2.7 |
| Streamer event | 0.3 | 5.4 | 9.2 | 5.1 | 3.3 | 2.1 | 0.6 | 1.9 |
| Fan | 2.0 | 6.5 | 3.5 | 0.0 | 1.1 | 1.4 | 1.2 | 1.6 |
| TOTAL | 100% | 100% | 100% | 100% | 100% | 100% | 100% | 100% |

# TABLE 3: SMM Coronal Mass Ejection DESCRIPTORS

| | Percentage of All Features | | | | | | | |
|---|---|---|---|---|---|---|---|---|
| DESCRIPTOR | 1980 | 1984 | 1985 | 1986 | 1987 | 1988 | 1989 | TOTAL |
| Prominence | 7.9 | 2.2 | 1.1 | 2.0 | 5.5 | 8.0 | 7.4 | 6.8 |
| Concave-Outward | 6.2 | 9.8 | 6.9 | 9.2 | 3.8 | 5.2 | 5.0 | 5.6 |
| Flat-Topped | 4.3 | 0.0 | 2.3 | 6.1 | 2.7 | 2.1 | 2.1 | 2.5 |
| Light-bulb | 1.6 | 3.3 | 1.1 | 3.1 | 1.1 | 1.2 | 0.8 | 1.3 |
| Halo | 0.0 | 1.1 | 1.1 | 0.0 | 0.0 | 0.5 | 0.7 | 0.5 |
| TOTAL | 20.0% | 16.4% | 12.5% | 20.4% | 13.1% | 17.0% | 16.0% | 16.7% |

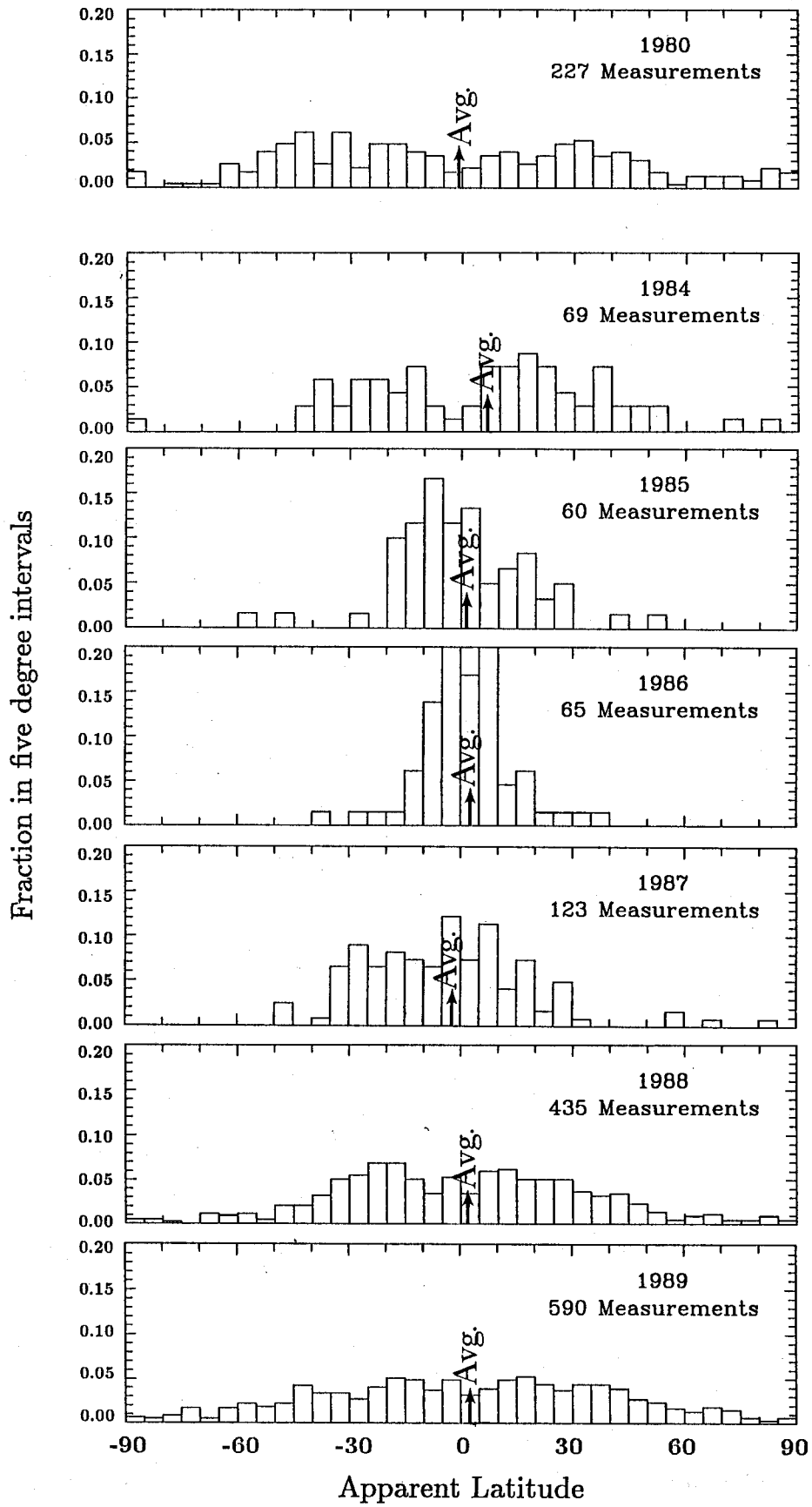


FIGURE 1. Distributions of apparent latitudes of coronal mass ejections from the Solar Maximum Mission Coronagraph/Polarimeter data set. All identified and measured features from each event are included. Average values are indicated for each year and given, along with the standard deviations in Table 1.

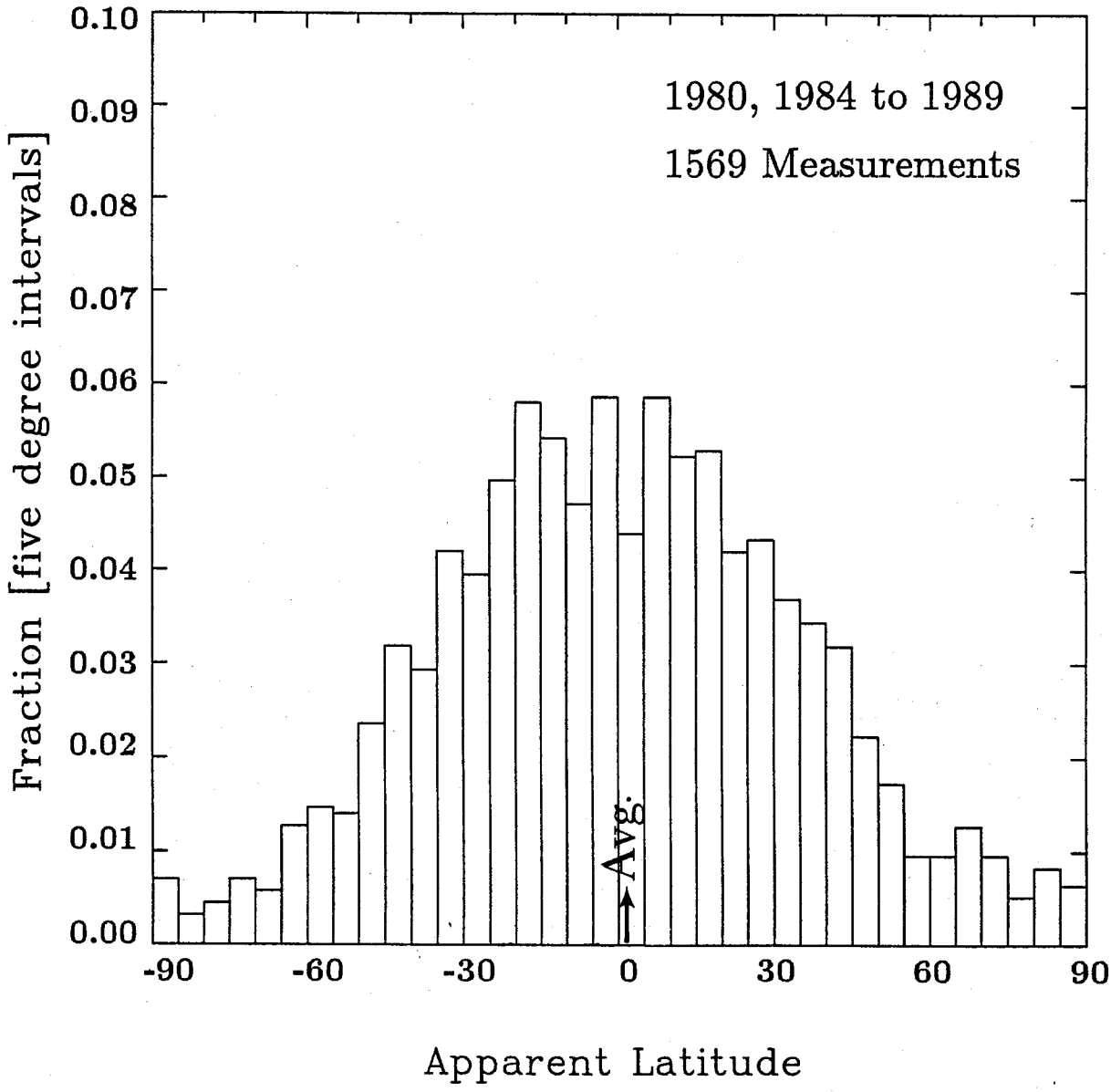


FIGURE 2. Distribution of apparent latitudes of coronal mass ejections for 1980 and 1984 through 1989 from the Solar Maximum Mission Coronagraph/ Polarimeter data set. The average value is indicated. All identified and measured features from each event are included.

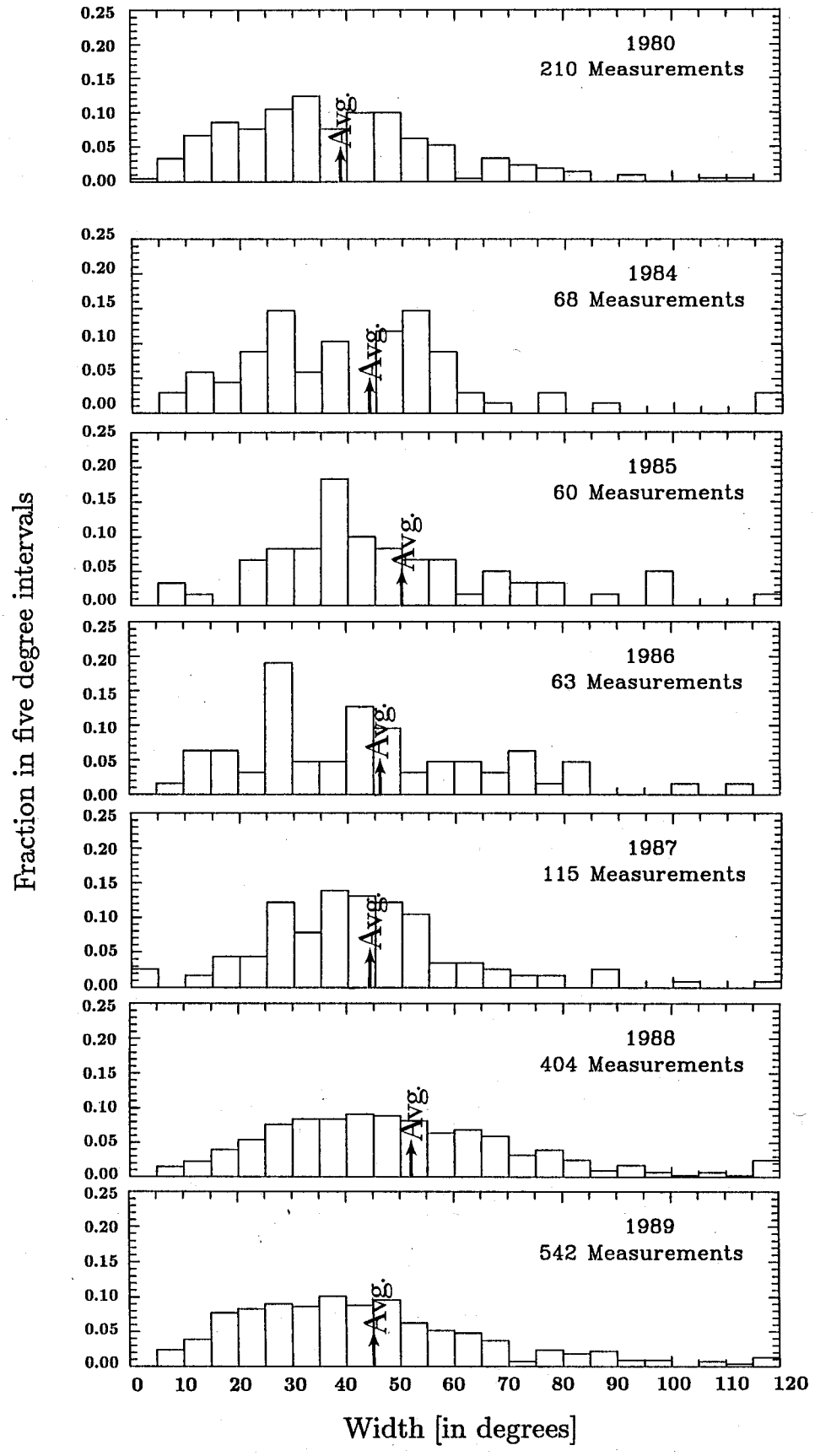


FIGURE 3. Distributions of apparent widths of coronal mass ejections from the Solar Maximum Mission Coronagraph/Polarimeter data set. All identified and measured features from each event are included. Average values are indicated for each year and given, along with medians in Table 1. The last bin contains all widths greater than 115 degrees.

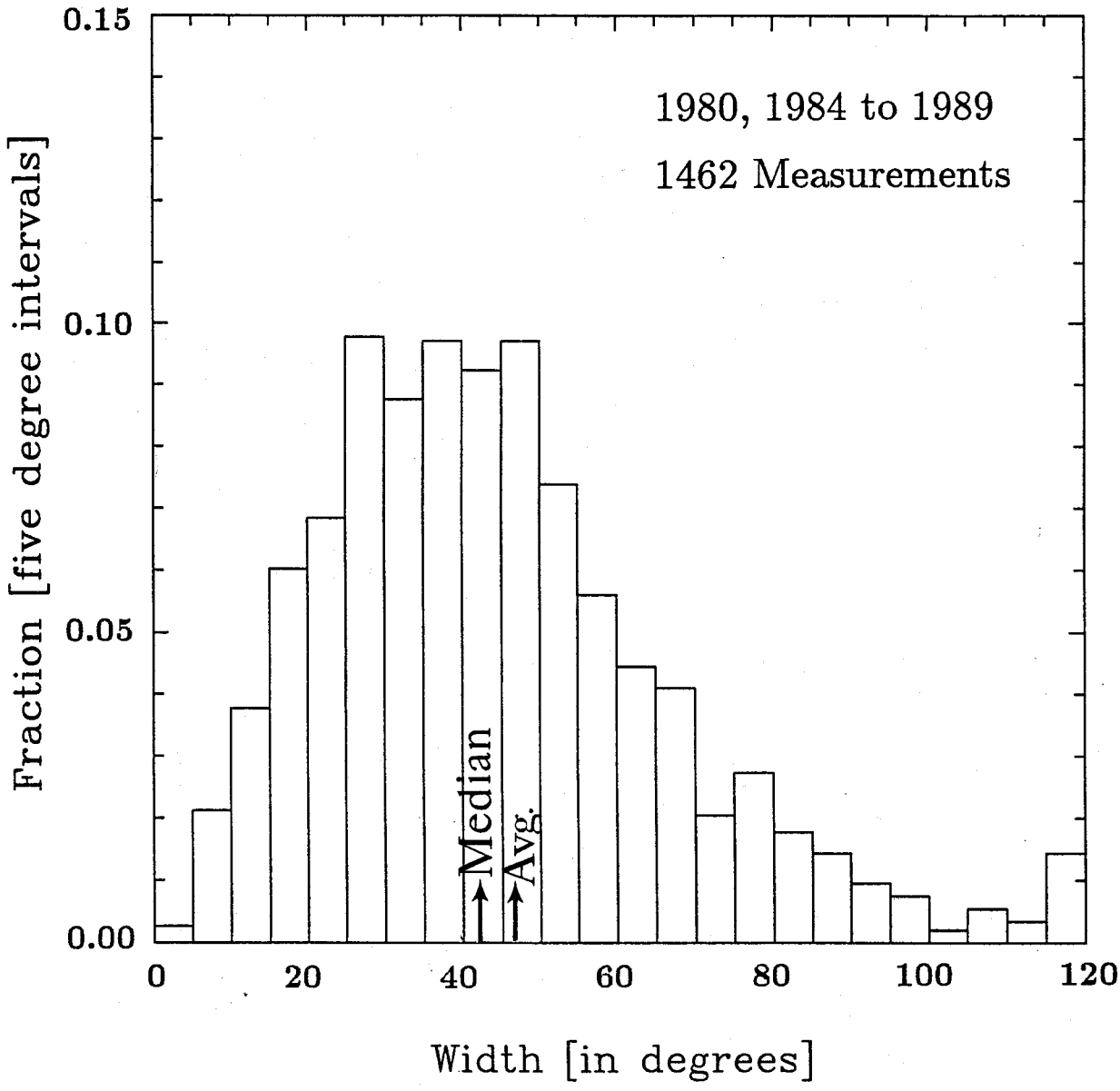


FIGURE 4. Distribution of apparent widths of coronal mass ejections for 1980 and 1984 through 1989 from the Solar Maximum Mission Coronagraph/ Polarimeter data set. Average and median values are indicated. All identified and measured features from each event are included. The last bin contains all widths greater than 115 degrees.

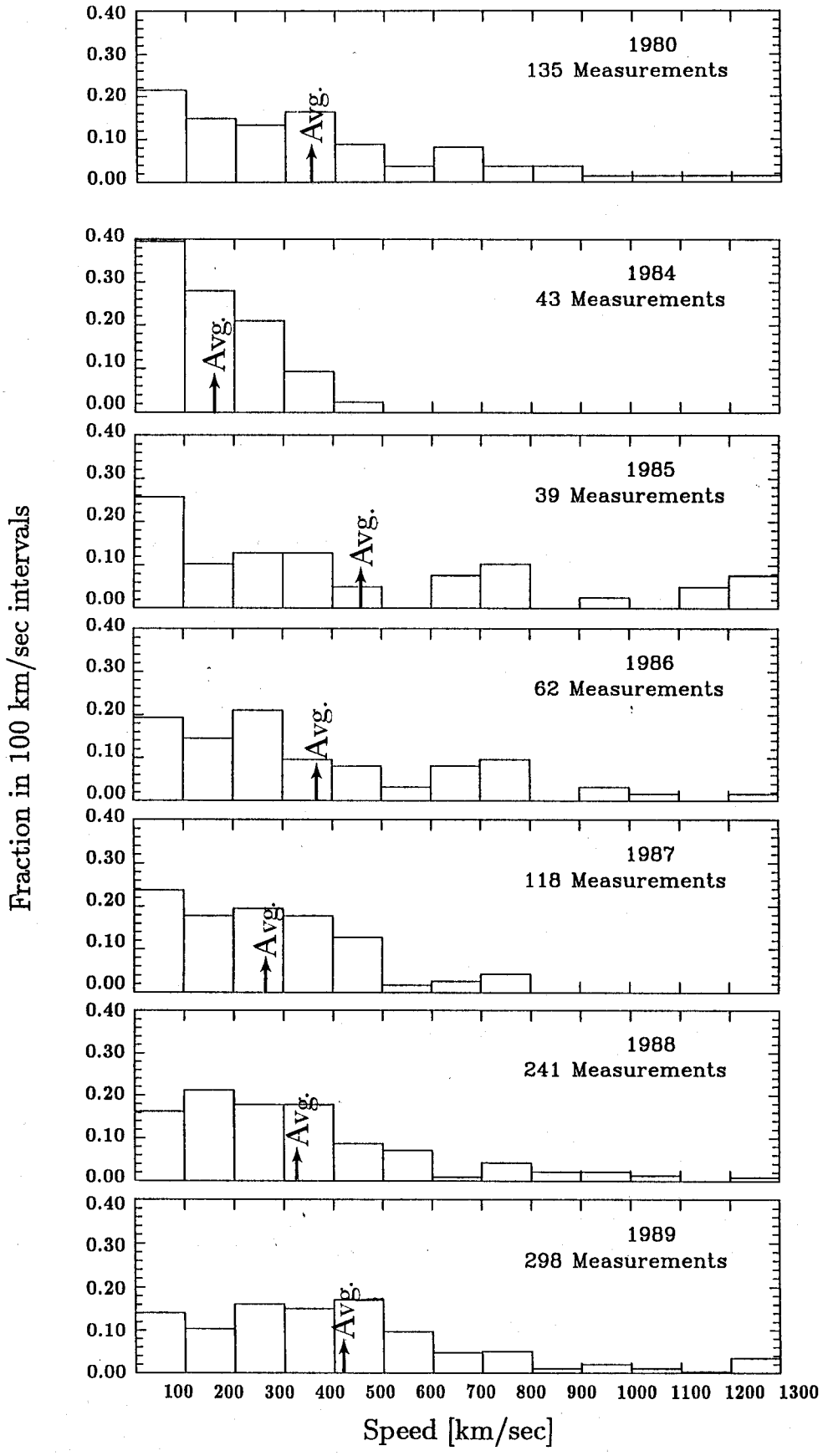


FIGURE 5. Distributions of apparent speeds of coronal mass ejections from the Solar Maximum Mission Coronagraph/Polarimeter data set. All identified and measured features from each event are included. Average values are indicated for each year and given, along with medians in Table 1. The last bin contains all speeds greater than 1200 km/sec.

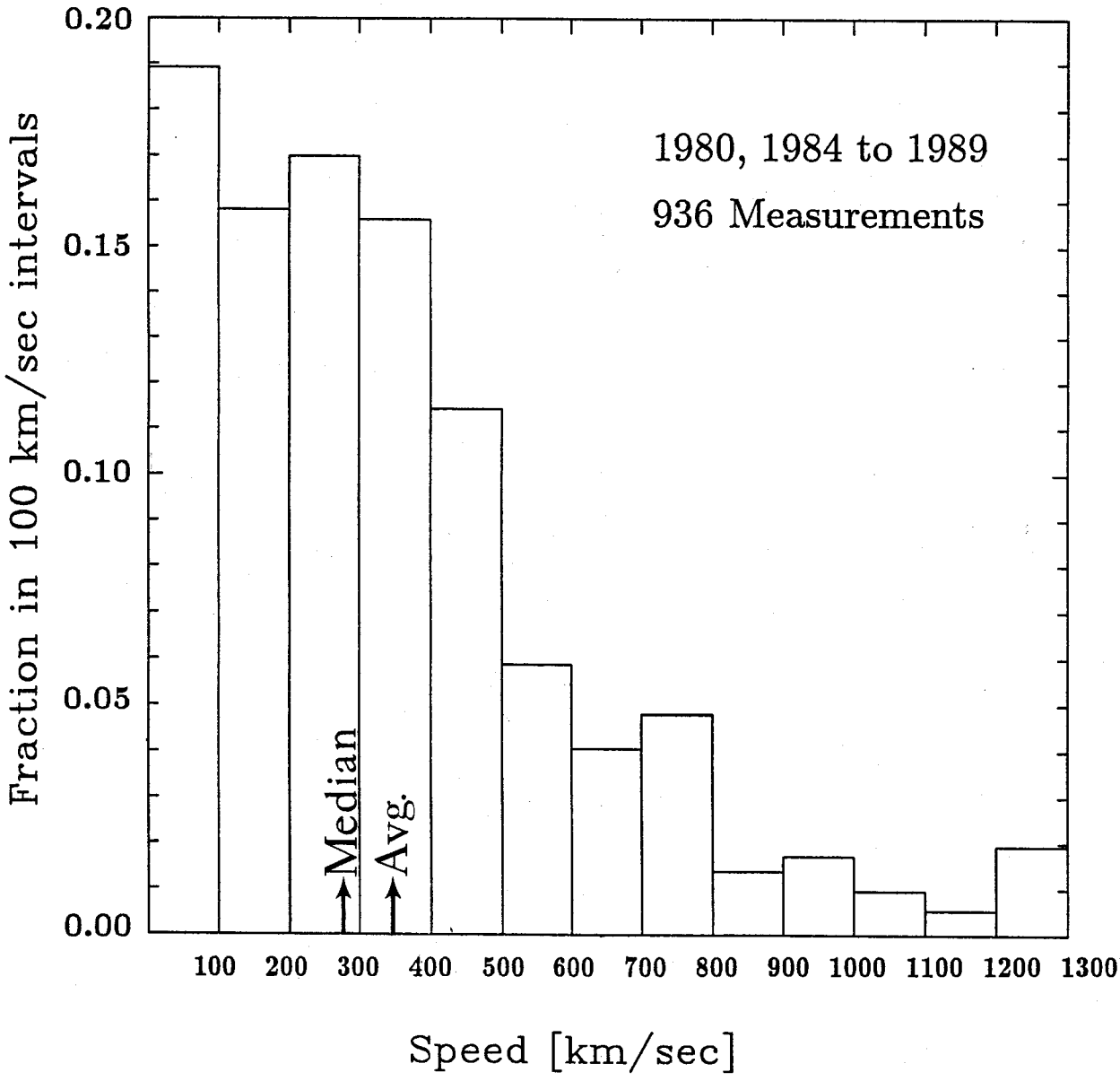


FIGURE 6. Distribution of apparent speeds of coronal mass ejections for 1980 and 1984 through 1989 from the Solar Maximum Mission Coronagraph/ Polarimeter data set. Average and median values are indicated. All identified and measured features from each event are included. The last bin contains all speeds greater than 1200 km/sec.

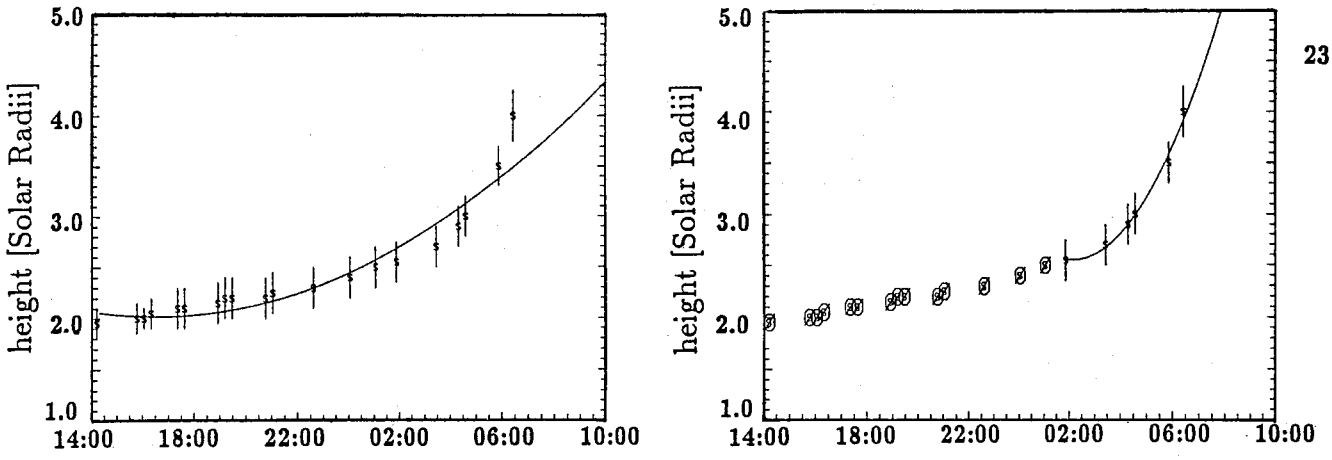


FIGURE 7a. Trajectories of cavity from Jan 9, 1988 at 124 degrees. Due to acceleration late in the event, the early data points were eliminated to get a better estimate of the final speed. The trajectory on the right is the 'preferred' fit.

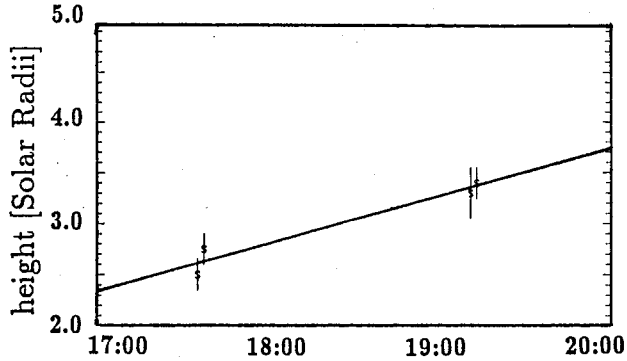


FIGURE 7b. Trajectory of cavity from Jul 16, 1980 at 225 degrees. No final speed from a second order fit was reported for this feature. Although more than two data points were available, the data were clumped in time behaving like a two point fit.

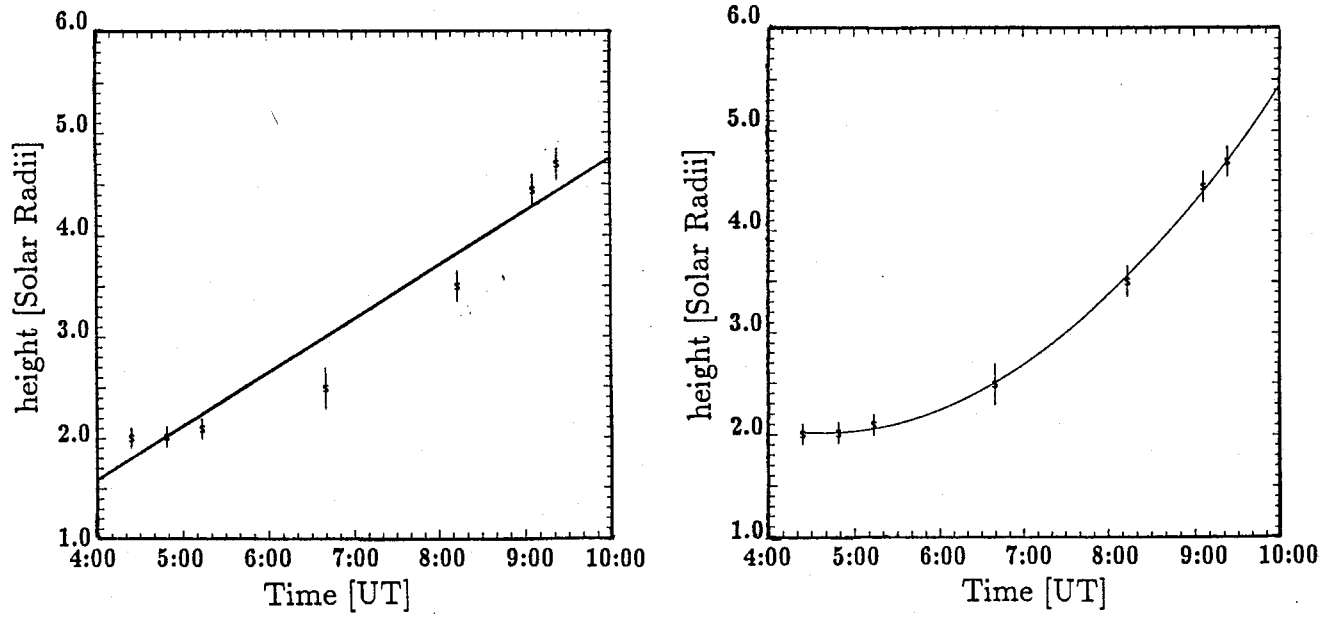


FIGURE 7c. Trajectories of cavity from Jun 1, 1988 at 298 degrees. No first order speed was reported for this feature. Due to acceleration, the first order trajectory (on the left) was a poor fit to the data. The second order trajectory (on the right) is the 'preferred' fit.

## VII. MORPHOLOGY PHOTOGRAPHS

Photographs of various morphologies, descriptors, and phenomena such as disruptions, appear on pages 25 through 53. Unless noted as a subtraction, all pictures are direct images of the corona and are a summation of vignetted K- and F-Corona plus stray light. In subtraction images, the red colored material represents a brightening due to the addition of, or compression of material from the pre-event image time. Blue areas indicate a deficit, or depletion of material from the pre-event time.

The coronagraph photos are all single sector images with the exception of the halo photograph on page 36. Here, four single sector images have been digitally combined to generate a full view of the corona.

In all images, an arrow indicates solar north, the dotted circle represents the solar photosphere, and the dash across the dotted circle marks the solar equator. The occulting disk obscures the inner corona out to ~1.6 solar radii. Some images contain a vertical bar in the center, a diagonal line to the upper left corner, and a black dot in the lower left corner. These marks are electronic artifacts and appear in most of the images.

Additional information on coronagraph images is available upon request.

SEP 14, 1988 SUBTRACTION
04:39 MINUS 01:39

JUN 4, 1989 SUBTRACTION
08:40 MINUS 07:07

FIGURE 8a: Two examples of the LOOP/CAVITY morphology.

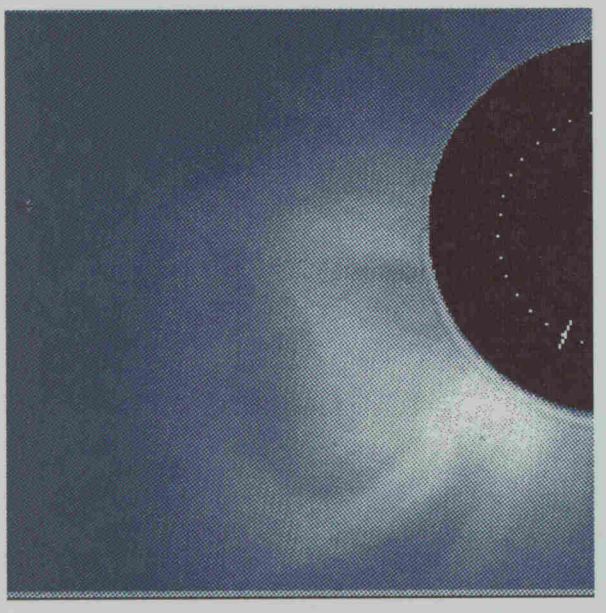

JUN 18, 1980 21:55

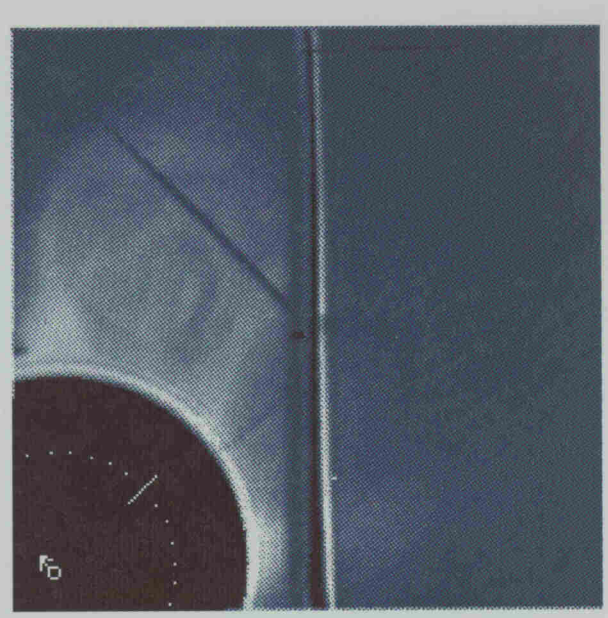

NOV 9, 1988 12:48

FIGURE 8b: Two examples of MULTIPLE LOOPS/CAVITIES .

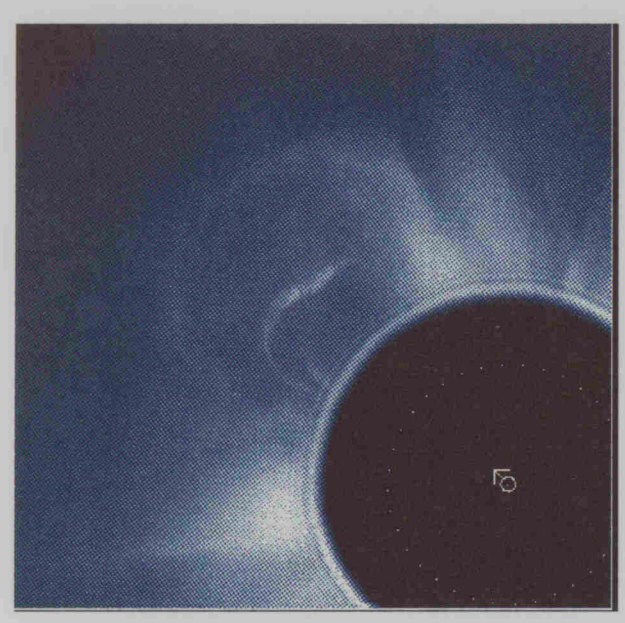

APR 14, 1980 05:44

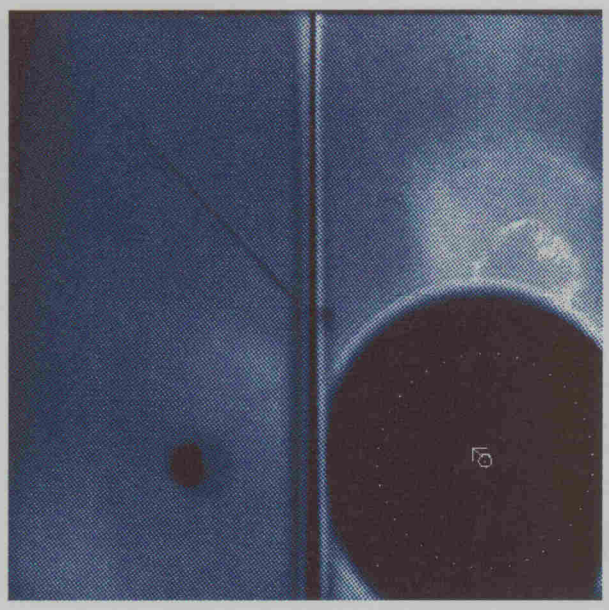

JAN 30, 1989 02:11

FIGURE 9a: Two examples of a CORONAL LOOP/Inner PROMINENCE LOOP

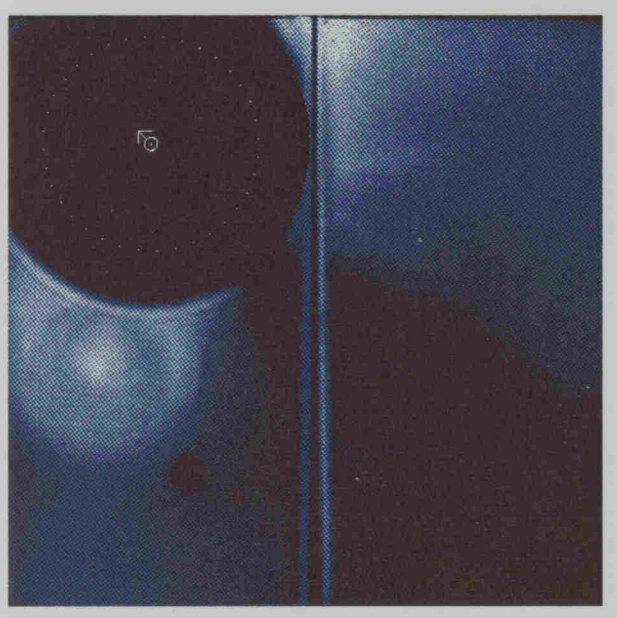

JAN 19, 1989 01:43

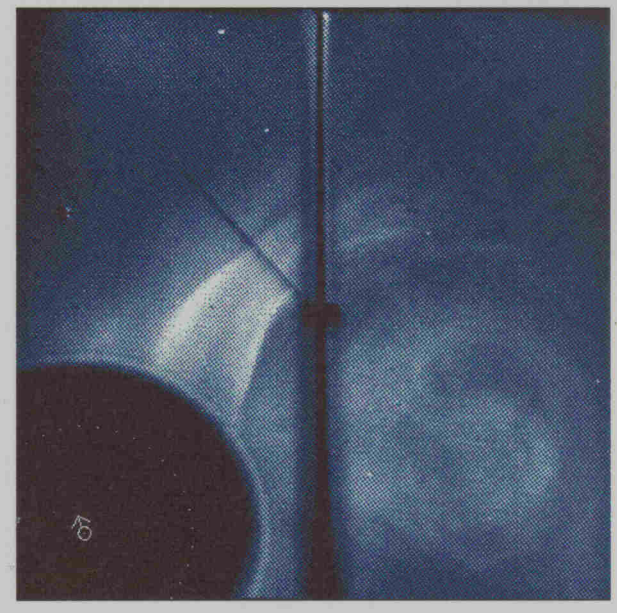

AUG 16, 1989 01:28

FIGURE 9b: Two examples of CORES embedded in the cavity trailing a loop front.

APR 30, 1980 SUBTRACTION
11:52 MINUS 10:21

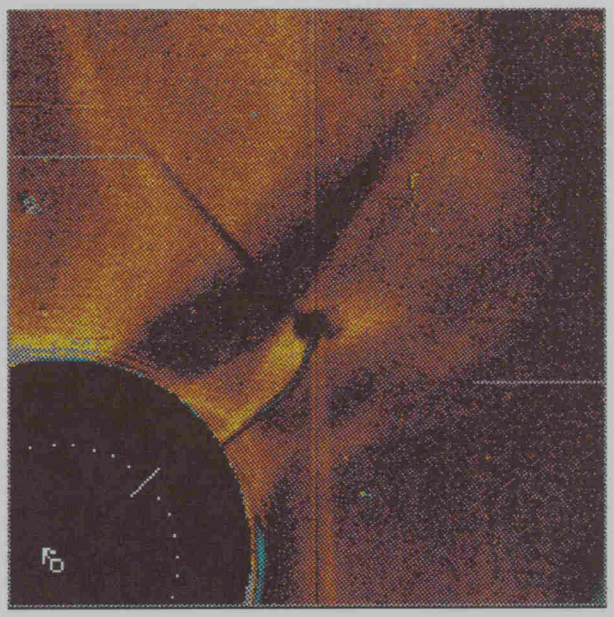

NOV 3, 1986 SUBTRACTION
20:38 MINUS 19:14

FIGURE 10a: Two examples of the CLOUD morphology.

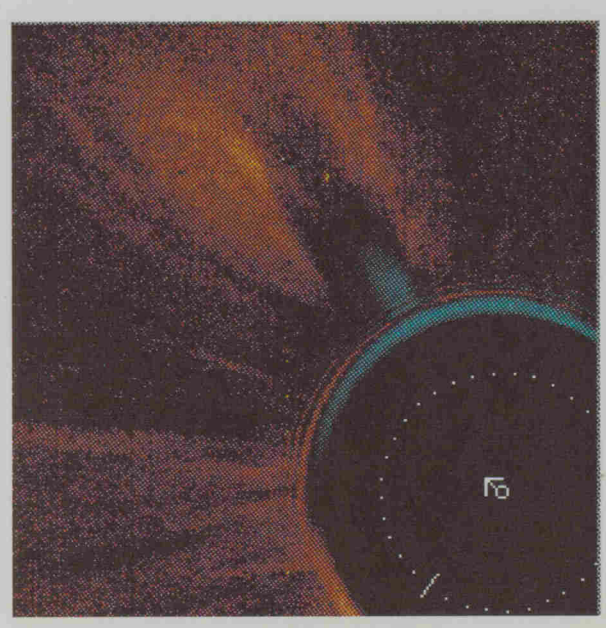

MAR 29, 1980 SUBTRACTION
07:22 MINUS 00:57

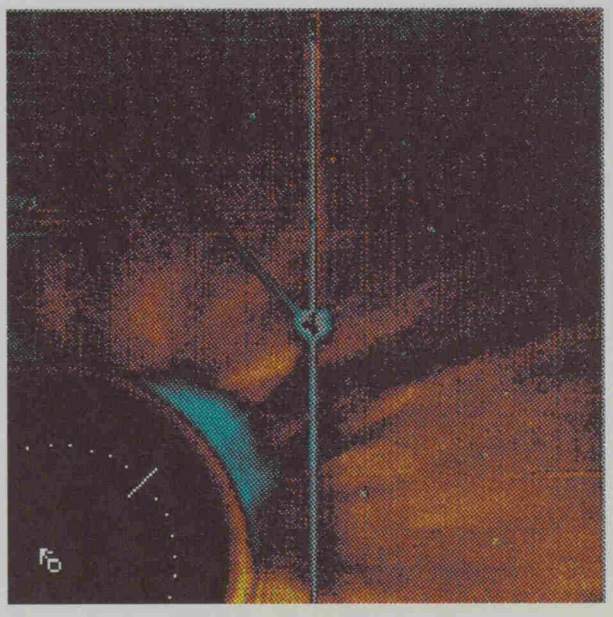

JUL 21, 1980 SUBTRACTION
06:12 MINUS JUL 20 20:27

FIGURE 10b: Two examples of GENERIC MATERIAL.

JAN 17, 1985 SUBTRACTION
18:06 MINUS 10:16

AUG 2, 1988 SUBTRACTION
20:09 MINUS 17:46

**FIGURE 11a: Two examples of the MOUND morphology.**

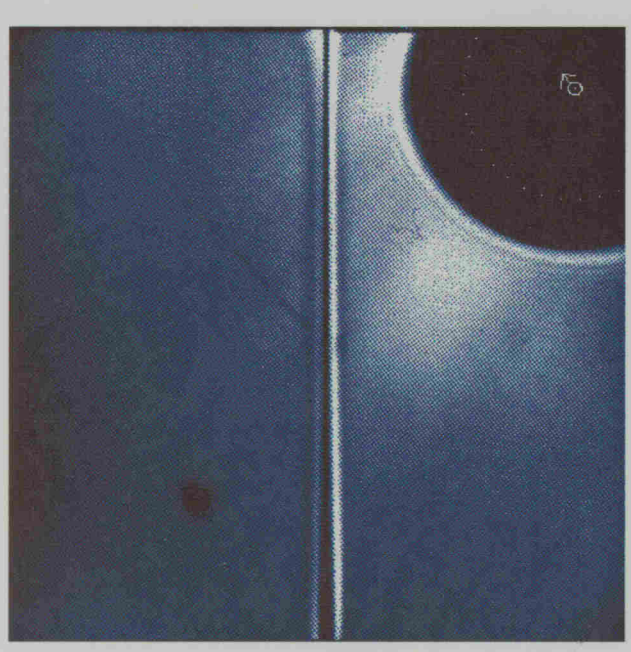

NOV 20, 1987 02:59

NOV 20, 1987 04:00

**FIGURE 11b: Two successive images of a CAVITY WITH NO VISIBLE LOOP FRONT. It is possible the loop has yet to form or it is too faint to be seen.**

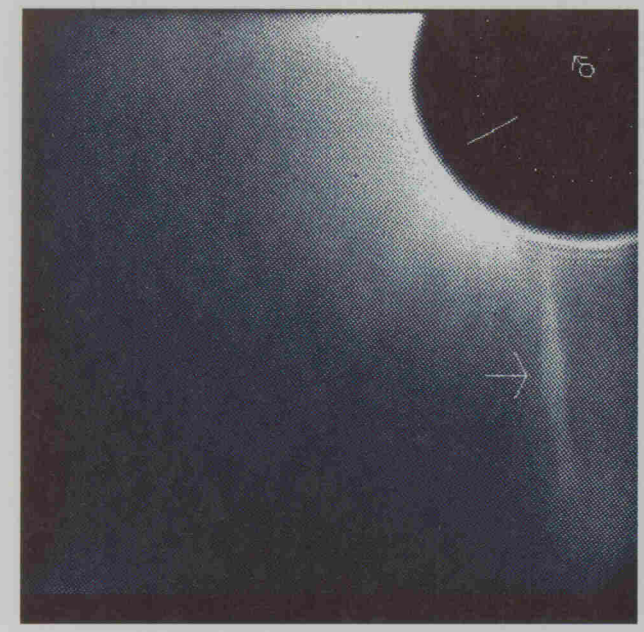

MAR 20, 1980 15:40

APR 18, 1987 SUBTRACTION
03:57 MINUS 02:23

FIGURE 12a: Two examples of the BLOB morphology.

NOV 10, 1986 SUBTRACTION
17:46 MINUS 16:40

AUG 23, 1988 SUBTRACTION
09:17 MINUS 08:00

FIGURE 12b: Two examples of the JET morphology.

MAY 20, 1988 SUBTRACTION
12:02 MINUS 10:12

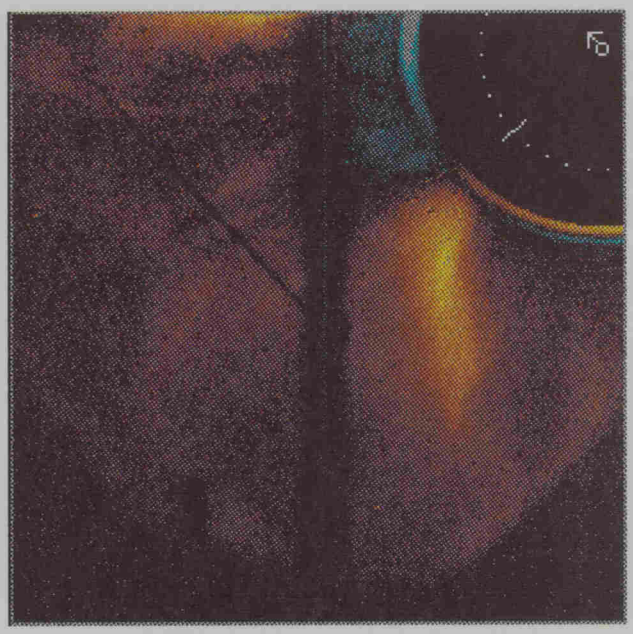

DEC 16, 1988 SUBTRACTION
09:06 MINUS 08:33

FIGURE 13a: Two examples of the TONGUE morphology.

OCT 21, 1987 SUBTRACTION
09:40 MINUS 02:21

JUL 11, 1988 SUBTRACTION
00:40 MINUS JUL 10 21:32

FIGURE 13b: Two examples of the FAN morphology.

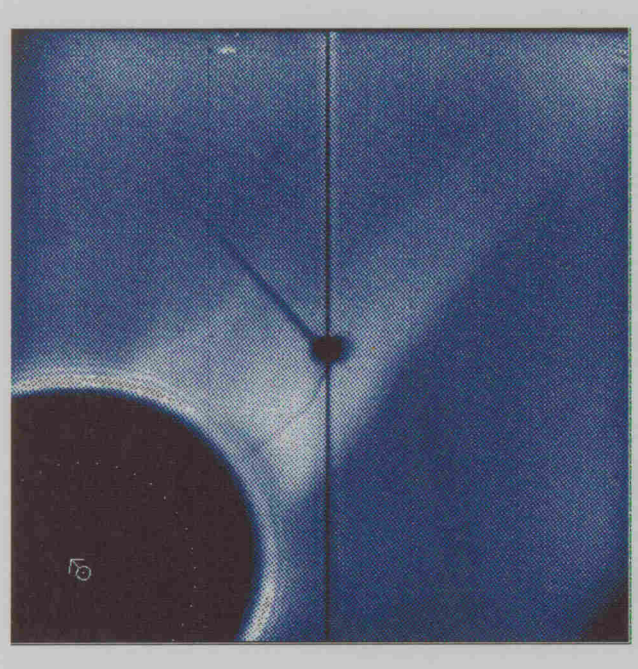

MAR 14, 1985 03:05

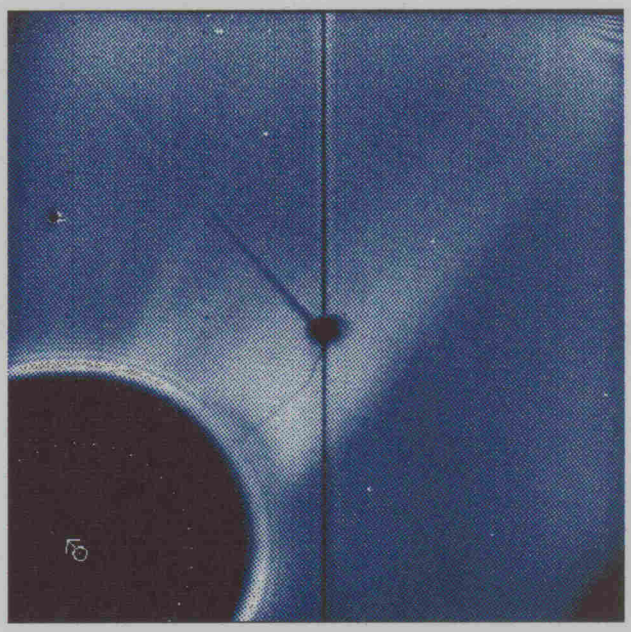

MAR 14, 1985 18:30

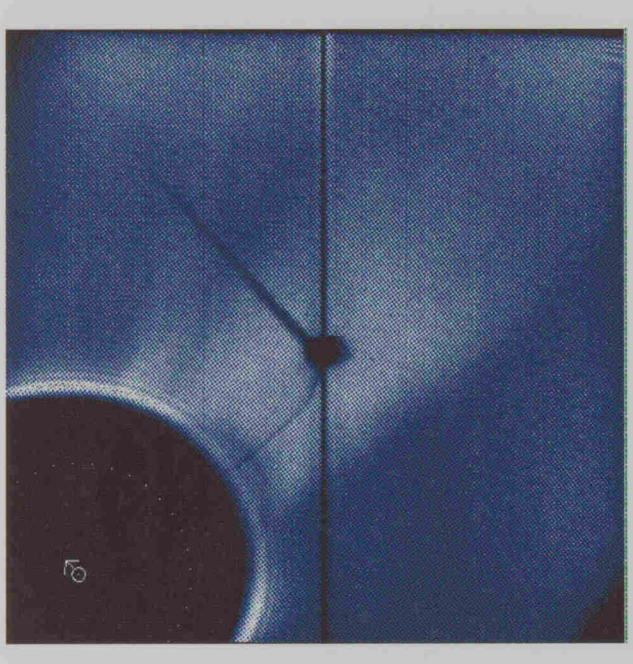

MAR 14, 1985 21:39

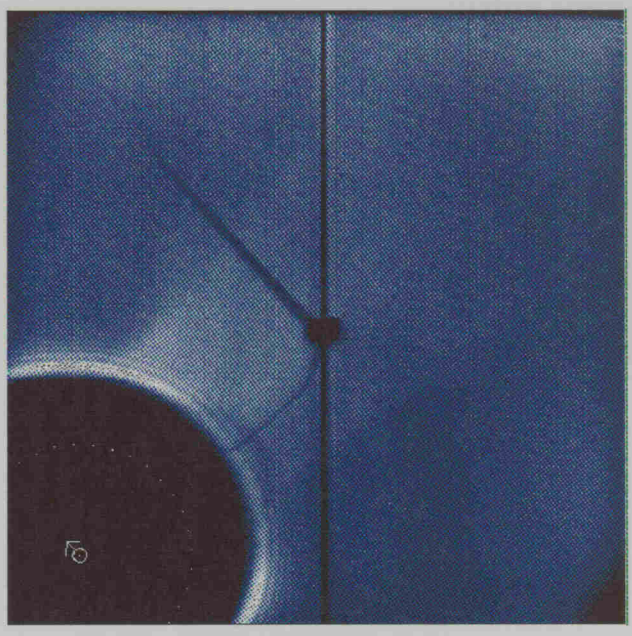

MAR 15, 1985 04:15

**FIGURE 14: STREAMER EVENT.** The helmet streamer, visible at 03:05 on Mar 14, slowly disrupts and blows out by Mar 15 04:15.

AUG 18, 1980 13:09

FEB 6, 1988 15:30

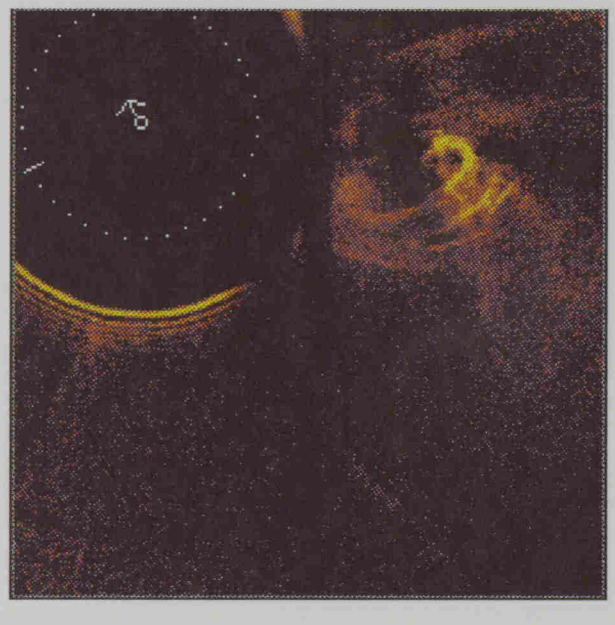

MAY 4, 1988 SUBTRACTION
06:08 MINUS 04:33

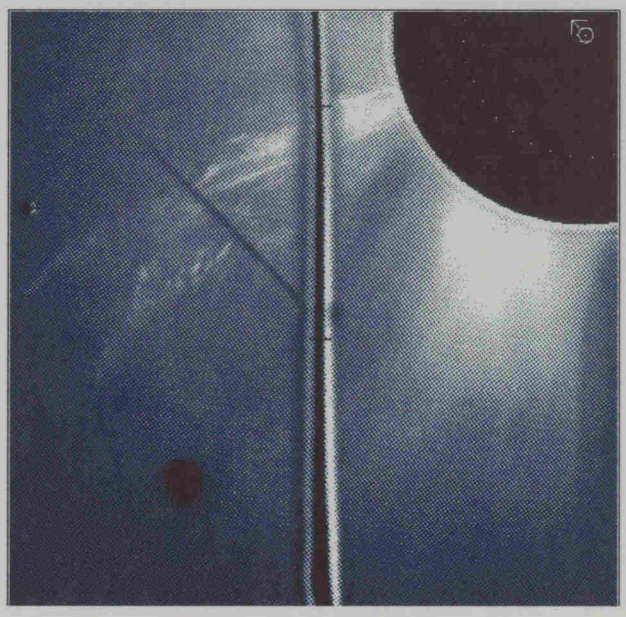

NOV 10, 1988 07:00

**FIGURE 15: A sample of some of the prettier PROMINENCES seen by the Solar Maximum coronagraph.**

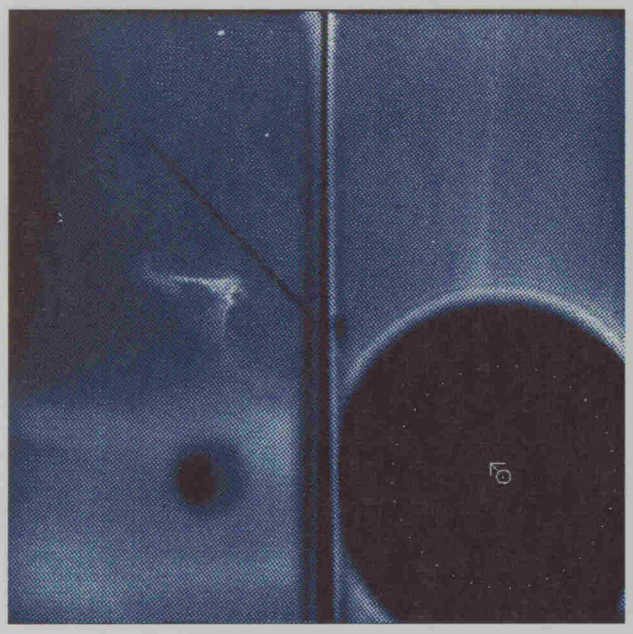

JAN 15, 1989 22:21

MAR 26, 1989 SUBTRACTION
17:56 MINUS 12:00

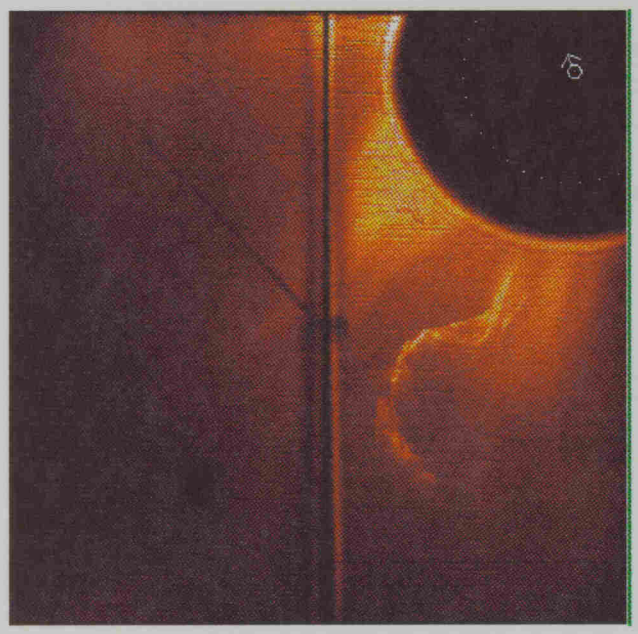

APR 23, 1989 10:16

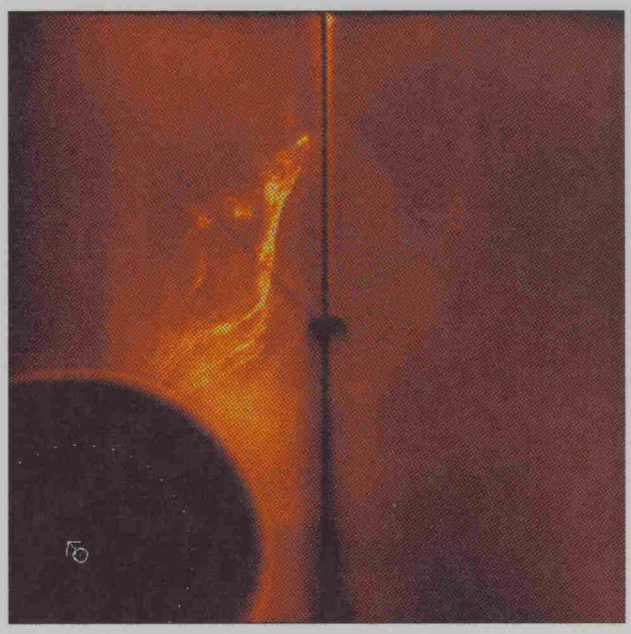

OCT 5, 1989 18:21

FIGURE 16: More examples of PROMINENCE material.

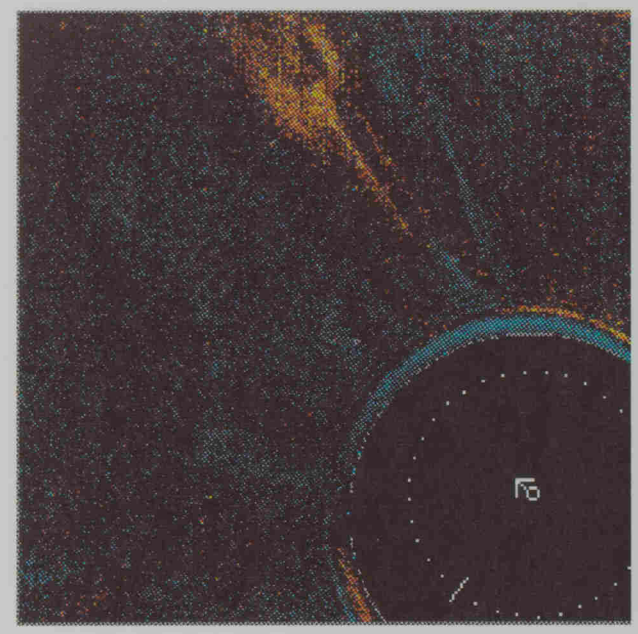

APR 5, 1980 SUBTRACTION
15:45 MINUS 13:48

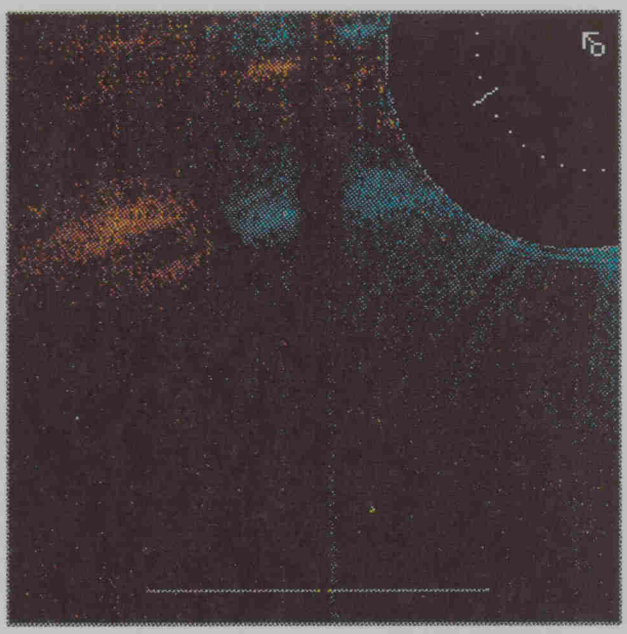

JUN 27, 1988 SUBTRACTION
23:05 MINUS 16:49

U-SHAPED

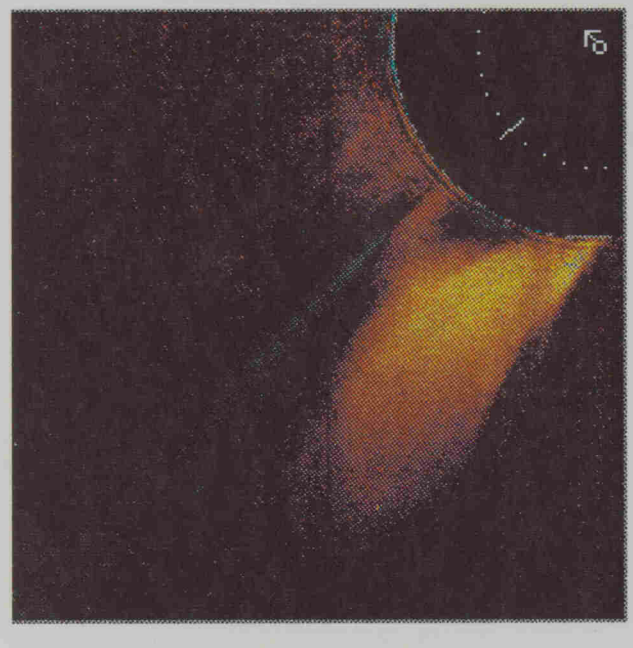

OCT 3, 1984 SUBTRACTION
03:35 MINUS OCT 2 13:25

JAN 8, 1989 SUBTRACTION
03:43 MINUS 02:53

V-SHAPED

FIGURE 17: Four examples of CONCAVE-OUTWARD geometry.

OCT 6, 1988 SUBTRACTION
19:13 MINUS 18:03

NOV 10, 1988 SUBTRACTION
11:41 MINUS 10:24

FIGURE 18a: Two examples of FLAT-TOPPED features.

OCT 18, 1984 SUBTRACTION
09:36 MINUS 02:21

DEC 10, 1984 SUBTRACTION
01:43 MINUS DEC 9 22:34

FIGURE 18b: Two examples of LIGHT BULBS.

MAR 23, 1989
NORTH: 21:19 MINUS 18:12
SOUTH: 21:27 MINUS 18:20

FOUR QUADRANT SUBTRACTION
EAST: 21:43 MINUS 18:37
WEST: 21:10 MINUS 18:47

FIGURE 19: Possible HALO. The pylon shadow, in the lower right corner of the image, obscures a wedge of approximately 40 degrees centered on the southern solar pole.

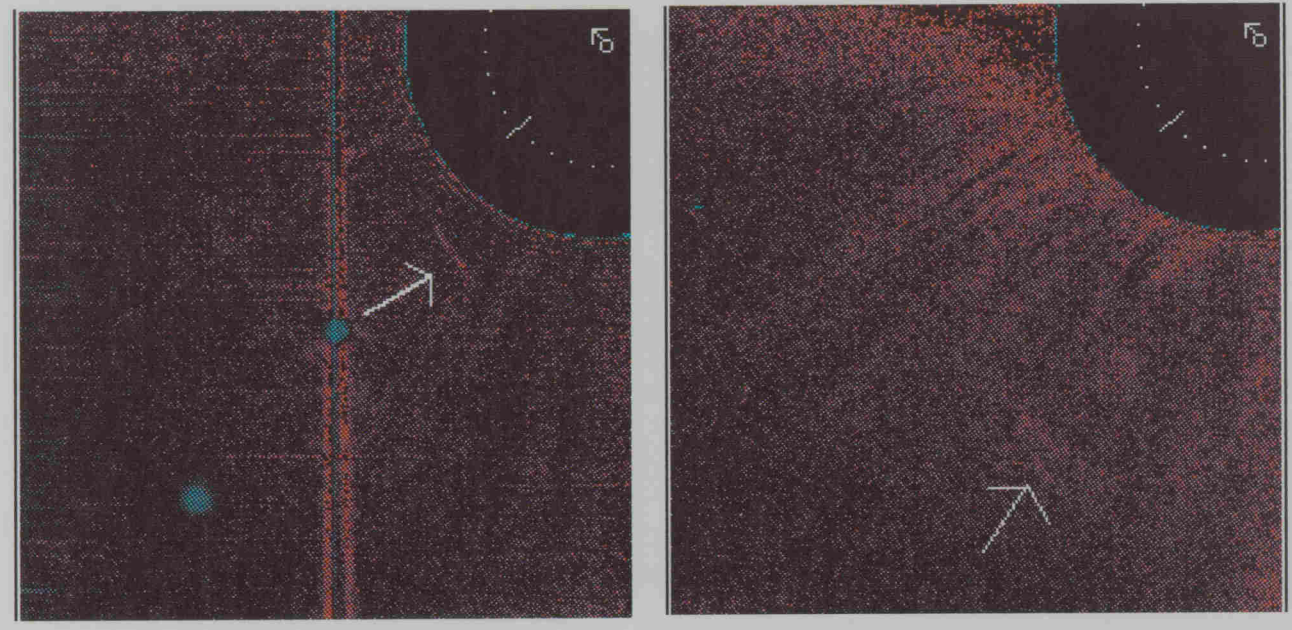

JUN 21, 1980 SUBTRACTION
23:15 MINUS 20:11

JUN 22, 1980 SUBTRACTION
00:51 MINUS JUN 21 20:11

FIGURE 20a: Two successive images of a VERY FAINT loop front.

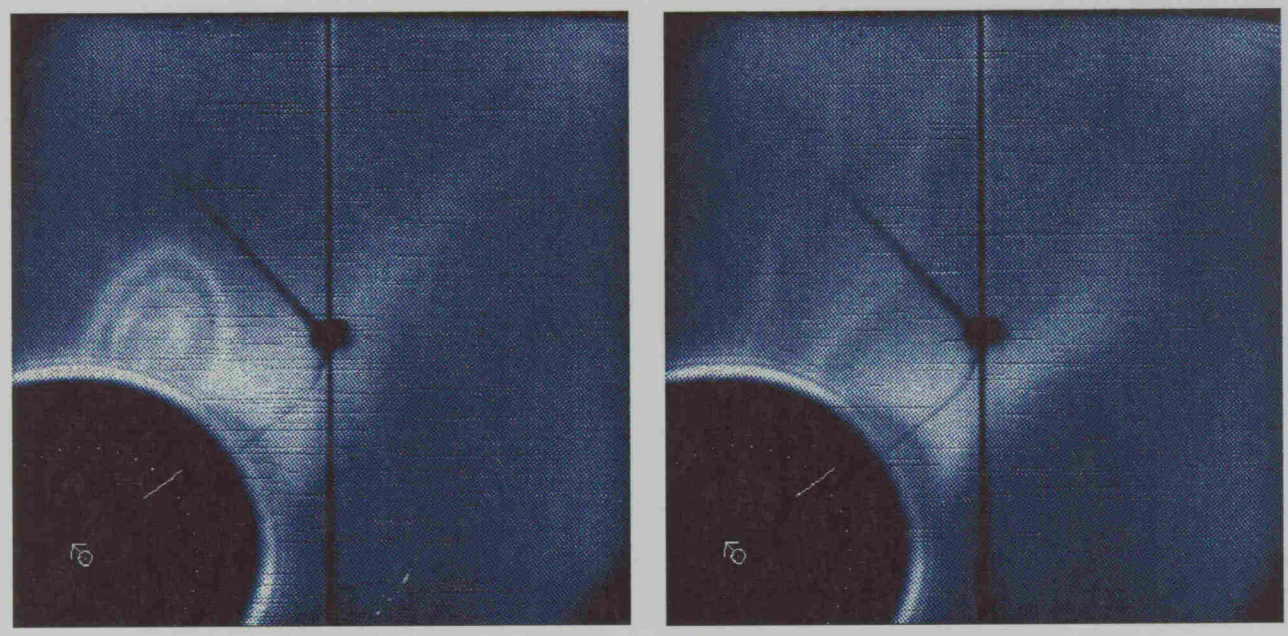

OCT 15, 1986 21:17

OCT 15, 1986 22:18

FIGURE 20b: DEFLECTION of a pre-existing helmet streamer by the passage of an event. The streamer was deflected southward between 21:17 and 22:18.

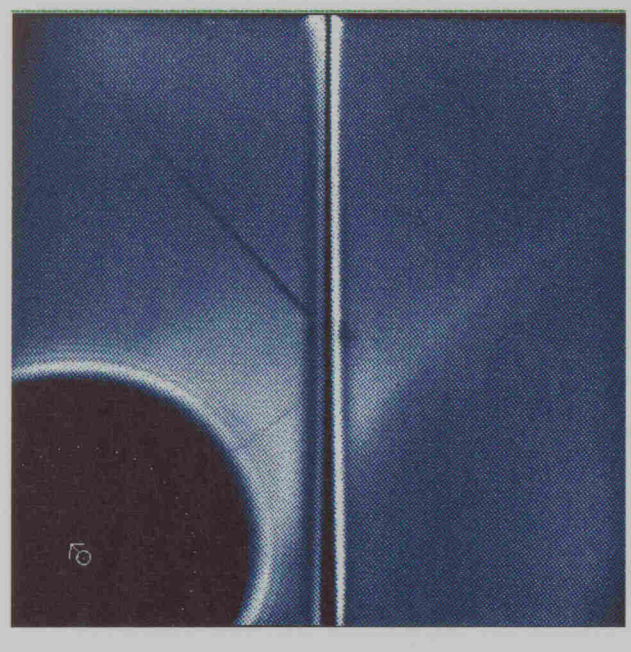

NOV 10, 1987 20:13

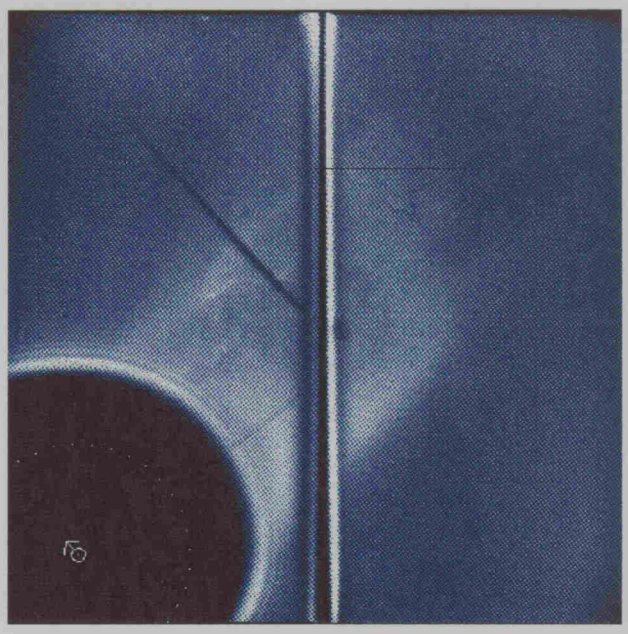

NOV 10, 1987 23:14

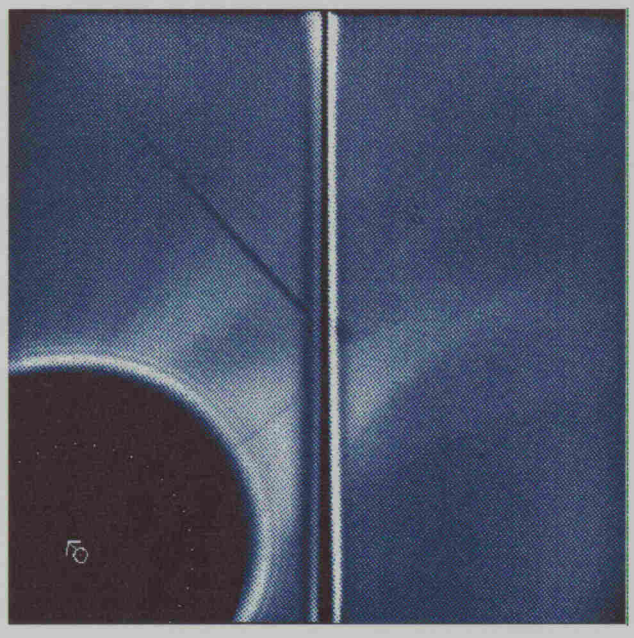

NOV 11, 1987 00:48

**FIGURE 21:** **PRE-EXISTING STRUCTURES ARE DISRUPTED** by the passage of an event. The background coronal material, visible in the image at 20:13, is disrupted by the event at 23:14. Some of the material has been shifted or removed by 00:48.

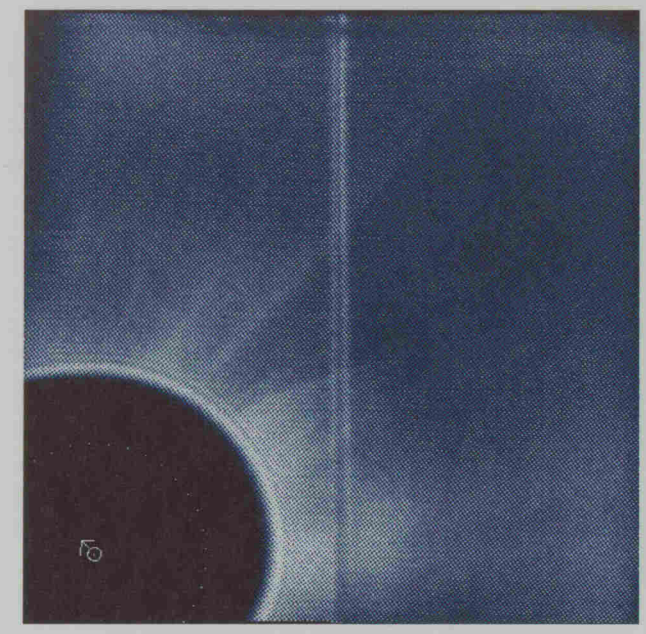

OCT 24, 1989 15:23

OCT 24, 1989 18:09

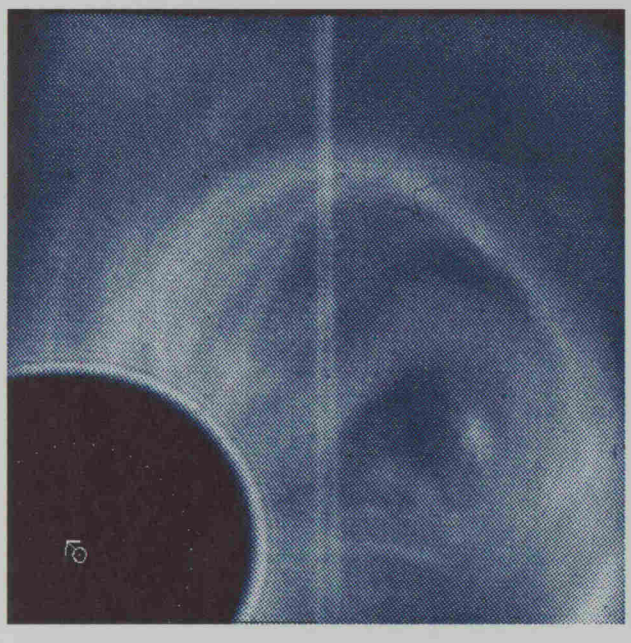

OCT 24, 1989 18:25

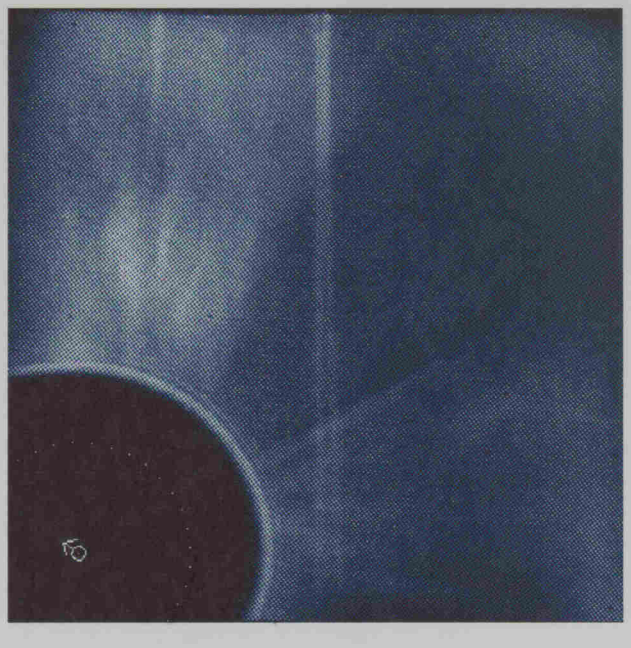

OCT 24, 1989 19:15

**FIGURE 22: PRE-EXISTING STRUCTURES ARE BLOWN OUT by the passage of an event. The coronal material, visible above the occulting disk in the lower right center of the image at 15:23, is blown out by 19:15 due to the loop/cavity appearing in the intervening images.**

## VIII. NOTE

In spite of significant proof-reading efforts, the authors suspect that any catalogue this size will contain errors. Any researcher wishing to use information contained within this list is urged to contact an HAO representative, so that specific measurements for a given event can be confirmed (and qualified, if necessary) and a suitable context for the event can be described. Such requests may be addressed to:

Dr. A. J. Hundhausen
High Altitude Observatory
P.O. Box 3000
Boulder, CO 80307

## IX. ACKNOWLEDGMENTS

We gratefully acknowledge the contributions of the many individuals who designed, constructed, administered and operated the coronagraph and the SMM spacecraft. The HAO data analysis effort has been led by A. J. Hundhausen, the Principal Investigator for the coronagraph. His guidance and active participation in all aspects of the analysis made this catalogue possible. Andrew Stanger has contributed software expertise and continuity to the project, and we are especially appreciative of his fine work. The authors gratefully acknowledge A. J. Hundhausen's and A. Stanger's valuable comments and suggestions on the text.

We recognize the efforts of R. MacQueen and L. House, the former Principal Investigators of the coronagraph. Others who have significantly contributed to the SMM project while at HAO include: R. H. Lee, R. Reynolds, S. Beck, D. Kobe, M. De La Pena, M. Rainey, and P. Reppert. We are very grateful to S. Paswaters and M. Hoswell who independently reviewed the entire data set from 1984 through 1986, discovering over 30 new mass ejections.

Student assistants who have worked on various aspects of the operations, analysis, and archiving since 1984 include: A. Gross, K. Walsh, S. Rosenberg, T. Warner, C. Waugh, S. Paswaters, M. Hoswell, J. Wong, S. Serbicki and M. Dodge. We thank Liz Boyd for assistance in the final preparation of this manuscript.

The SMM coronagraph program was funded principally by the National Aeronautics and Space Administration Contract Number S-04167D.

## X. REFERENCES

Hildner, E., Gosling, J.T., Hansen, R.T. and Bohlin, J.D., "The sources of material comprising a mass ejections coronal transient." *Solar Physics*, **45**, 363-376, 1975.

Howard, R.A., D.J. Michels, N.R. Sheeley, and M.J. Koomen, "The observation of a coronal transient directed at the Earth." *Astrophys J.*, **263**, L101-L104, 1982.

Howard, R.A., N.R. Sheeley, M.J. Koomen, and D.J. Michels, "Coronal Mass Ejections." *J. Geophys. Res.*, **90**, No. A9, 8173-8191, 1985.

Hundhausen, A.J., "The sizes and locations of coronal mass ejections: SMM observations from 1980 and 1984-1989." accepted for publication by *J. Geophys. Res.*, 1993.

———— T.E. Holzer, and B.C. Low, "Do slow shocks precede some coronal mass ejections?", *J. Geophys. Res.*, **92**, 173, 1987.

———— C.B. Sawyer, L. House, R.M.E. Illing, and W.J. Wagner, "Coronal mass ejections observed during the *Solar Maximum Mission*: Latitude distribution and rate of occurrence." *J. Geophys. Res.*, **89**, No. A5, 2639-2646, 1984.

Illing, R.M.E. and A.J. Hundhausen, "Possible observation of a disconnected magnetic structure in a coronal transient." *J. Geophys. Res.*, **88**, 10210-10214, 1983.

Kahler, S., "Coronal mass ejections." *Reviews of Geophysics*, **25**, 663-675, 1987.

MacQueen, R.M., A. Csoeke-Poeckh, E. Hildner, L.L. House, R. Reynolds, A. Stanger, H. TePoel, and W.J. Wagner, "The High Altitude Observatory coronagraph/polarimeter on the *Solar Maximum Mission*", *Solar Physics*, **65**, 91-107, 1980.

————- and O.C. St.Cyr, "Sungrazing comets observed by the *Solar Maximum Mission* coronagraph", *Icarus*, **90**, 96-106, 1991.

McComas, D. J., J. L. Phillips, A. J. Hundhausen, and J. T. Burkepile, "Disconnection of Open Coronal Magnetic Structures," in *Geophysical Research Letters*, **18**, 73-76, 1991.

Munro, R.H., J.T. Gosling, E. Hildner, R.M. MacQueen, A.I. Poland, and C.L. Ross, "The association of coronal mass ejection transients with other forms of solar activity." *Solar Physics*, **61**, 201-215, 1979.

——— and D.G. Sime, "White Light Coronal Transients Observed from *Skylab* May 1973 to February 1974: A Classification by Apparent Morphology." *Solar Physics*, **97**, 191-201, 1985.

Schmahl, E. and Hildner, E., "Coronal mass ejections kinematics of the 19 December 1973 event." *Solar Physics*, **55**, 473-490, 1977.

St.Cyr, O. C. and Burkepile, J.T., "A Catalogue of Mass Ejections Observed by the *Solar Maximum Mission* Coronagraph", National Center for Atmospheric Research Technical Note NCAR/TN-352+STR July 1990.

Webb, D.F. and E. W. Cliver, "Disconnections in Coronal Mass Ejections," *Bull. AAS*, 21, 857, 1989.

Woodgate, B.E. and S.P. Maran, "The *Solar Maximum Mission* repair–lessons learned", Space Station Automation II, SPIE Conference Proc.,729, 202, 1986.

# A revised and expanded catalogue of mass ejections observed by the solar maximum mission coronagraph. - Link Page

Next PART0002